

```
double precision, intent(inout) :: ep  
double precision, intent(out) :: f  
double precision :: c, H  
integer, intent(out) :: region, error
```

```
if (this%s_type==1) then
```

# Elasto-Plastic Strain Hardening Mohr-Coulomb Model

Derivation and Implementation into the Finite Element Model using Principal Stress Space

```
    RETURN
```

```
else if (this%s_type==2 .or. this%s_type==3) then
```

```
    allocate(A(4,4))
```

```
else if (this%s_type==4) then
```

```
    allocate(A(6,6))
```

```
end if
```

```
call this%getch(ep, c, H)
```

```
call toprincipal(sigb, sigbp, A, s_typein=this%s_type)
```

```
region=0
```

```
f=this%k*sigbp(1,1)-sigbp(3,1)-2*c*sqrt(this%k)
```

```
if (f > 0) then
```

```
    call this%getregion(sigbp, ep, region)
```

```
end if
```

```
select case(region)
```

```
case(0)
```

```
    sigcp=sigbp
```

```
case(1)
```

```
    call this%returntoMCP(sigbp, ep, sigcp, error)
```

```
    call this%DepcMCP(sigbp, sigcp, ep, Depcp)
```

```
case(2)
```

```
    call this%returntoMCL1(sigbp, ep, sigcp, error)
```

```
    call this%DepcMCL1(sigbp, sigcp, ep, Depcp)
```

```
case(3)
```

```
    call this%returntoMCL6(sigbp, ep, sigcp, error)
```

```
    call this%DepcMCL6(sigbp, sigcp, ep, Depcp)
```

```
case(4)
```

```
    call this%returntoMCS(sigbp, ep, sigcp, error)
```

```
    call this%DepcMCS(sigbp, sigcp, ep, Depcp)
```

```
end select
```

```
call fromprincipal(sigcp, sigc, A, Depcp, Depc, s_typein=this%s_type)
```

```
end subroutine update
```

```
subroutine getregion(this, sigb, ep, region)
```

```
    implicit none
```

```
    class(MohrCoulomb) :: this
```

```
    double precision, dimension(3,1), intent(in) :: sigb
```

```
    double precision, intent(out) :: region
```

```
    double precision, dimension(4,1) :: BPeval
```

```
    double precision :: c, H, apex
```

```
    integer, intent(out) :: region
```

```
    call this%getch(ep, c, H)
```

```
    apex=2*c*sqrt(this%k)/(this%-1)
```

```
    BPeval(1,1)=dot_product(this%nL1(:,1),sigb(:,1)-apex)
```

```
    BPeval(2,1)=dot_product(this%nL6(:,1),sigb(:,1)-apex)
```

Emil Smed Sørensen, Aalborg University

M.Sc. 4th Semester, 8 June 2012



**School of Engineering  
and Science**

Sohngårdsholmsvej 57

Telefon 96 35 97 31

Fax 98 13 63 93

<http://ses.aau.dk>

## **Summary:**

**Title:** Elasto-plastic Hardening Mohr-Coulomb Model - Derivation and Implementation into the Finite Element Method Using Principal Stress Space

**Theme:** Master Thesis

**Project period:** M.Sc. 4th semester, spring 2012

**Project group:** B124C

**Participants:**

---

Emil Smed Sørensen

**Supervisor:** Johan Clausen

**Circulation:** 3

**Number of pages:** 70

**Submitted:** 8th of June 2012

The purpose of this report is to derive and implement a strain hardening Mohr-Coulomb model based on return mapping in principal stress space by the use of boundary planes. The report aims at modeling strain hardening rock material through a Mohr-Coulomb approximation of the generalized Hoek-Brown criterion. Firstly, the classification of rock materials as well as the generalized Hoek-Brown criterion are presented. Afterwards follows an introduction to the Mohr-Coulomb criterion and the approximations used for the generalized Hoek-Brown criterion.

Next, the fundamentals of plasticity and hardening is presented along with the theory behind return mapping in general stress space, including the derivation of the consistent constitutive matrix used in the global FEM equilibrium iterations. Then the advantages of return mapping in principal stress space is outlined. Following is the derivation of a non-associated isotropic strain hardening Mohr-Coulomb model based on the introduced theory.

Finally, the derived model is implemented in two examples. The first example tries to model a strip footing while the second example models a tunnel excavation. The obtained results are compared with perfectly plastic solutions utilizing the peak and residual strength of the rock material.



---

# Contents

<b>1</b>	<b>Introduction</b>	<b>1</b>
1.1	Statement of Intent . . . . .	3
1.2	Prerequisites . . . . .	3
<b>2</b>	<b>Classification of Rock Materials and the Generalized Hoek-Brown Criterion</b>	<b>5</b>
<b>3</b>	<b>The Mohr-Coulomb Criterion</b>	<b>9</b>
3.1	Mohr-Coulomb Approximation of Hoek-Brown criterion . . . . .	10
<b>4</b>	<b>Plasticity Fudamentals</b>	<b>13</b>
4.1	The Yield Function . . . . .	13
4.2	Plastic Potential . . . . .	15
4.3	Hardening and Softening . . . . .	15
4.4	State Parameters . . . . .	16
4.5	Time-Independency . . . . .	17
4.6	Infinitesimal Constitutive Matrix . . . . .	17
4.7	Multiple Yield Functions . . . . .	18
<b>5</b>	<b>Return Mapping in General Stress Space</b>	<b>21</b>
5.1	Non-linear Finite Element Method . . . . .	21
5.2	Return Mapping Basics . . . . .	22
5.3	Return to One Active Yield Function . . . . .	24
5.4	Return to Two Active Yield Functions . . . . .	25
5.5	Return to Three Active Yield Functions . . . . .	28
5.6	Determination of Correct Return Type . . . . .	28
<b>6</b>	<b>Return Mapping in Principal Stress Space</b>	<b>29</b>
6.1	Modificaton Matrix . . . . .	30
6.2	Boundary Planes . . . . .	31
<b>7</b>	<b>Implementation of Strain Hardening Mohr-Coulomb Model</b>	<b>33</b>
7.1	Basic Premises . . . . .	33

7.2	Derivatives . . . . .	33
7.3	Yield Criterion Regions . . . . .	34
7.4	Return Regions and Boundaries . . . . .	36
7.5	Return Algorithms . . . . .	38
7.6	Consistent Constitutive Matrix . . . . .	41
<b>8</b>	<b>Computational Example: Strip Footing</b>	<b>43</b>
8.1	The Model . . . . .	43
8.2	Material Parameters . . . . .	44
8.3	Mesh Coarseness . . . . .	45
8.4	Results . . . . .	45
<b>9</b>	<b>Computational Example: Tunnel Excavation</b>	<b>51</b>
9.1	The model . . . . .	51
9.2	Material Parameters . . . . .	52
9.3	Mesh Coarseness . . . . .	53
9.4	Results . . . . .	53
<b>10</b>	<b>Conclusion</b>	<b>59</b>
	<b>Bibliography</b>	<b>61</b>

---

# Introduction

A large part of the earth's crust consists of material which can be classified as rock. With advances within the field of civil engineering and the ever growing need for real estate and infrastructure, more and more structures are built in or on rock material. For some civil engineering structures, this is a major advantage, since rock material is often very strong and stiff. Properties which are beneficial for a foundation. However, rock material also tends to be quite brittle and possess inferior tensile strength. Properties, which are dangerous to tunnel excavations.

Civil engineering problems involving rock material, as well as many other problems, are often handled by the use of finite element modeling, where the generally non-linear governing equations of the model are discretized into a finite number of elements, for which the solution to the governing equations can be approximated with polynomials. Afterwards the system of equations is solved in an incremental iterative manner until equilibrium is reached. A crucial part in the finite element method is the choice of constitutive model, which gives the relationship between the strains and the stresses in a given point.

Part of the constitutive model is to predict when plastic straining of the material occurs, which is dictated by the yield criterion. For rock materials, two often used yield criteria are the old-fashioned and thoroughly tested Mohr-Coulomb criterion and the fairly new generalized Hoek-Brown criterion. The Mohr-Coulomb criterion describes a linear relationship between the shear stress in the material and the corresponding normal stress, which when satisfied, results in plastic straining of the material. The Hoek-Brown criterion is an empirical non-linear refinement of the Mohr-Coulomb criterion and is specifically designed for rock-like materials. However, due to the simplicity of the Mohr-Coulomb criterion, many calculations regarding rock-like material is still carried out using this simpler criterion.

Another part of the constitutive model is to predict how the material behaves under plastic straining. Generally, materials respond in three different ways, see Figure 1.1. One possibility is, that the material strengthens during plastic loading until some ultimate strength is reached, in which case the material is said to harden. Another possibility is, that the material maintains a constant strength, and the material is said to be perfectly plastic. The third possibility is, that the material has a peak strength, and weakens until a residual strength is reached, a phenomenon known as softening. The phenomenon of gaining or losing strength during plastic loading is sometimes referred to simply as hardening, regardless that the material is softening.

The rate of change of the strength of the material is also a significant factor, which has to be considered when modeling materials. The behavior of rock materials generally evolve in three possible ways. Hard, good quality rock material tends to show an elastic-brittle behavior, in which the strength drops

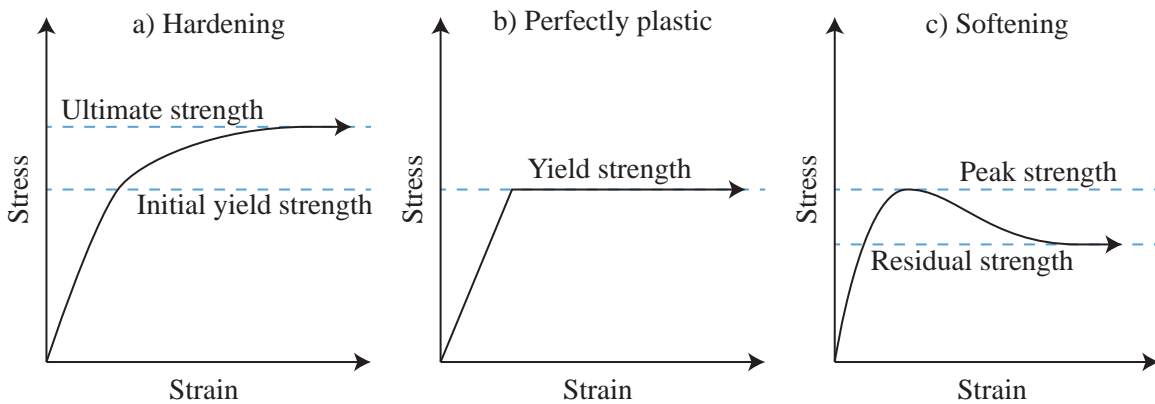


Figure 1.1: *Material behaviour under plastic loading.*

rapidly, once the material is introduced to plastic straining, see Figure 1.2. Average quality rock material tends to show a strain softening behavior similar to the one shown in Figure 1.1c, while very poor quality rock material shows an elastic-perfectly plastic behavior, see Figure 1.1b, [Hoek and Brown, 1997]. Many finite element models rely on the material to behave in a perfectly plastic manner with a

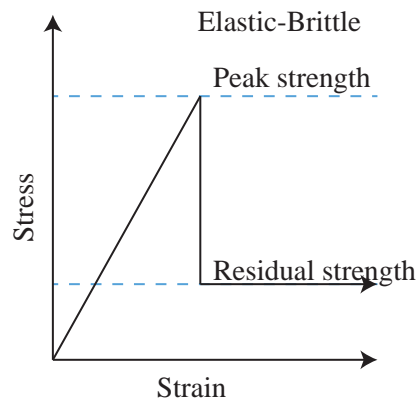


Figure 1.2: *Elastic-brittle behavior in hard rock material*

yield strength equivalent to the residual strength. This greatly reduces the problem and thus makes it easier to solve. However, it could also possibly lead to over sized structures if the material is softening, because local zones of high plastic straining dictate the strength of the entire material. For example if a perfectly plastic approach is used with a strength above the residual strength, material located in plastic zones is stronger than it should be, and hence the model is on the unsafe side. On the other hand, if the residual strength is used for the entire material, the model might be too conservative.

Constitutive models based on the Mohr-Coulomb criterion which include hardening/softening are already available, see e.g. de Souza Neto et al. [2008]. However, a model based on the principal stress space framework presented by Clausen [2007] has yet to be developed.

## 1.1 Statement of Intent

The aim of this project is to derive a strain hardening/softening constitutive model for use in finite element calculations based on the Mohr-Coulomb criterion which utilize derivations in principal stress space, both regarding the updated stress state and the consistent constitutive matrix needed for the global equilibrium iterations.

To test and demonstrate the usefulness of the model, it is used to estimate the influence of the hardening/softening properties on the bearing capacity of a strip footing as well as the risk of failure during a tunnel excavation.

## 1.2 Prerequisites

Strains and stresses are tensors of the 2nd order and the constitutive relation between them is a 4th order tensor. However, symmetric properties of the strain and stress tensors allow for a formulation in which they can be expressed equally accurate as vectors, and the constitutive relation can be expressed as a matrix. In this report, the latter formulation will be used due to its simplicity and ease of use when writing computer code. Throughout the report, a number of variables, vectors and matrices are used. To keep track of these, a number of guidelines will be presented in the following.

A scalar is presented in ordinary text as  $\sigma_1$ , whereas a vector or a matrix is symbolized in bold as e.g.  $\boldsymbol{\sigma}$  or  $\boldsymbol{D}$ . By default, vectors are  $6 \times 1$  and matrices are  $6 \times 6$ . Vectors and matrices with an overline, e.g.  $\overline{\boldsymbol{\sigma}}$  and  $\overline{\boldsymbol{D}}$  are related to the principal stress components and have dimensions of  $3 \times 1$  and  $3 \times 3$  respectively. Vectors and matrices with a tilde, e.g.  $\tilde{\boldsymbol{\sigma}}$  and  $\tilde{\boldsymbol{T}}$  are related to the shear stress components and have dimensions of  $3 \times 1$  and  $3 \times 3$  respectively. Vectors and matrices with a hat, e.g.  $\hat{\boldsymbol{\sigma}}$  and  $\hat{\boldsymbol{D}}$  are full  $6 \times 1$  vectors and  $6 \times 6$  matrices, where the axes are aligned with those of the principal stresses.

The ordering of the strain vector,  $\boldsymbol{\varepsilon}$ , and the stress vector,  $\boldsymbol{\sigma}$ , is given as

$$\boldsymbol{\varepsilon} = [\varepsilon_x \quad \varepsilon_y \quad \varepsilon_z \quad 2\varepsilon_{xy} \quad 2\varepsilon_{xz} \quad 2\varepsilon_{yz}]^T \quad (1.1)$$

$$\boldsymbol{\sigma} = [\sigma_x \quad \sigma_y \quad \sigma_z \quad \sigma_{xy} \quad \sigma_{xz} \quad \sigma_{yz}]^T \quad (1.2)$$

Stresses are taken as positive in tension unless otherwise stated.  $\boldsymbol{D}$  is the elastic constitutive matrix relating elastic strains to stresses and is given by

$$\boldsymbol{D} = \begin{bmatrix} \overline{\boldsymbol{D}} & \mathbf{0}_{3 \times 3} \\ \mathbf{0}_{3 \times 3} & \tilde{\boldsymbol{G}} \end{bmatrix} \quad (1.3)$$

where  $\overline{\boldsymbol{D}}$  and  $\tilde{\boldsymbol{G}}$  are given by

$$\overline{\boldsymbol{D}} = \frac{E}{(1+\nu)(1-2\nu)} \begin{bmatrix} 1-\nu & \nu & \nu \\ \nu & 1-\nu & \nu \\ \nu & \nu & 1-\nu \end{bmatrix} \quad (1.4)$$

$$\tilde{\boldsymbol{G}} = \frac{E}{2(1+\nu)} \begin{bmatrix} 1 & 0 & 0 \\ 0 & 1 & 0 \\ 0 & 0 & 1 \end{bmatrix} \quad (1.5)$$

$E$  is Young's modulus and  $\nu$  is Poisson's ratio.



# Classification of Rock Materials and the Generalized Hoek-Brown Criterion

Rock material is a wide expression used to describe a solid made up of minerals. Depending on the size of a rock sample, see Figure 2.1, rock material typically ranges from isotropic intact rock mass without any discontinuities, through very anisotropic rock mass with a few dominating discontinuities, to an isotropic jointed rock mass with an indistinct number of randomly oriented evenly space discontinuities with the same characteristics [Merifield et al., 2006].

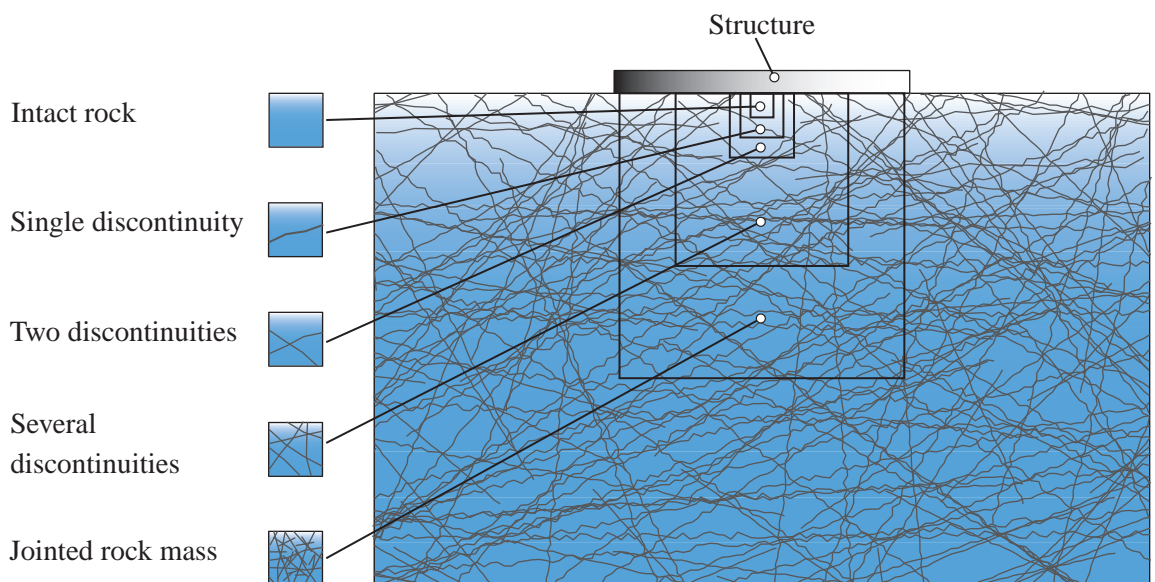


Figure 2.1: *The material which is modeled, should be isotropic compared to the size of the structure.*

If a representative sample of the rock material, which is sought modeled, can be regarded as either intact rock or as jointed rock mass, then the material can be regarded as isotropic, provided that the sample size is small compared to the structure at hand. If the discontinuities of the sample are oriented in a non-random order, it might be necessary to model the rock material as an anisotropic continuum. If large fractures(faults) dominate the construction site of the structure, it may also be necessary to include

such fractures in the model mesh. In the following, it is assumed, that the rock material can be modeled as an isotropic continuum.

In order to be able to include rock material in finite element models, the properties of the rock material need to be known and somehow quantified. Extensive empirical research has lead to the formulation of the generalized Hoek-Brown criterion, equation (2.1), which predict the stress states that cause failure in rock materials [Hoek and Brown, 1997].

$$\sigma'_1 = \sigma'_3 + \sigma_{ci} \left( m_b \frac{\sigma'_3}{\sigma_{ci}} + s \right)^a \quad (2.1)$$

$\sigma'_1$  and  $\sigma'_3$  are the major and minor effective principal stresses respectively, where compression is taken as positive. As the criterion suggests, four parameters are needed in order to asses the strength of the rock material, namely the uniaxial compressive strength of the intact rock material,  $\sigma_{ci}$ , and the constants  $m_b$ ,  $s$  and  $a$ . The constants can be estimated based on the Geological Strength Index(GSI), the disturbance factor,  $D$ , and the intact rock material constant,  $m_i$ , by using the following expressions [Hoek et al., 2002]

$$m_b = m_i \exp \left( \frac{GSI - 100}{28 - 14D} \right) \quad (2.2)$$

$$s = \exp \left( \frac{GSI - 100}{9 - 3D} \right) \quad (2.3)$$

$$a = \frac{1}{2} + \frac{1}{6} \left( \exp \left( \frac{-GSI}{15} \right) - \exp \left( \frac{-20}{3} \right) \right) \quad (2.4)$$

The Geological Strength Index is a measure of the rock material's quality based on field observations, which takes into account the composition and structure of the in-situ rock material as well as the surface conditions, see Figure 2.3 on page 8. Based on this, the GSI is assigned on a scale ranging from 0 to 100, where 100 indicates a very good quality [Hoek, 2007].

The disturbance factor,  $D$ , is used to take into account the blast damage, that part of the rock material might suffer from. It ranges from 0 to 1, where 0 indicates undisturbed rock material. The material constant  $m_i$  and the uniaxial compressive strength of the intact rock material,  $\sigma_{ci}$ , is found using laboratory tests on the intact rock material. The elastic modulus of the rock material can be estimated by [Hoek and Diederichs, 2006]

$$E_{rm} = 100,000 \text{ MPa} \left( \frac{1 - D/2}{1 + \exp((75 + 25D - GSI)/11)} \right) \quad (2.5)$$

Once the rock material has reached a stress state which causes failure, it loses some of its strength, as mentioned in chapter 1. The manner in which the strength drops is not entirely determined, but three possible characteristics are mentioned in Hoek and Brown [1997]. One possibility is to assume an elastic-brittle behavior, where the strength of the rock material rapidly drops to some residual strength once the failure criteria is reached, see Figure 1.2. Another possibility is to assume a strain softening relationship between the strength of the material and the plastic straining which it undergoes, see Figure 1.1c. The third options is to assume that the rock material exhibits in a elastic-perfectly plastic way, see Figure 1.1b. In this report, it is assumed that the rock material behaves in a strain-softening manner. For an implementation of an elastic-perfectly plastic generalized Hoek-Brown criterion see Clausen [2007] and Sørensen [2012].

In order to conform with most finite element codes, where tension is taken as positive, the generalised Hoek-Brown criterion can be expressed as

$$\sigma_3 = \sigma_1 - \sigma_{ci} \left( s - m_b \frac{\sigma_1}{\sigma_{ci}} \right)^a \quad (2.6)$$

where the apostrophes signifying effective stresses have been omitted for simplicity. In order to express the above as a yield function, resulting in a negative number for elastic states and a positive number for non-allowable states, it can further be rewritten to the following

$$f(\sigma, \sigma_{ci}, s, m_b, a) = \sigma_1 - \sigma_3 - \sigma_{ci} \left( s - m_b \frac{\sigma_1}{\sigma_{ci}} \right)^a = 0 \quad (2.7)$$

The stress states which are solutions to the above equation form a six sided pyramid along the hydrostatic axis with curved sides as can be seen in Figure 2.2. Any stress state inside the pyramid is elastic, whereas any stress state located outside is unobtainable.

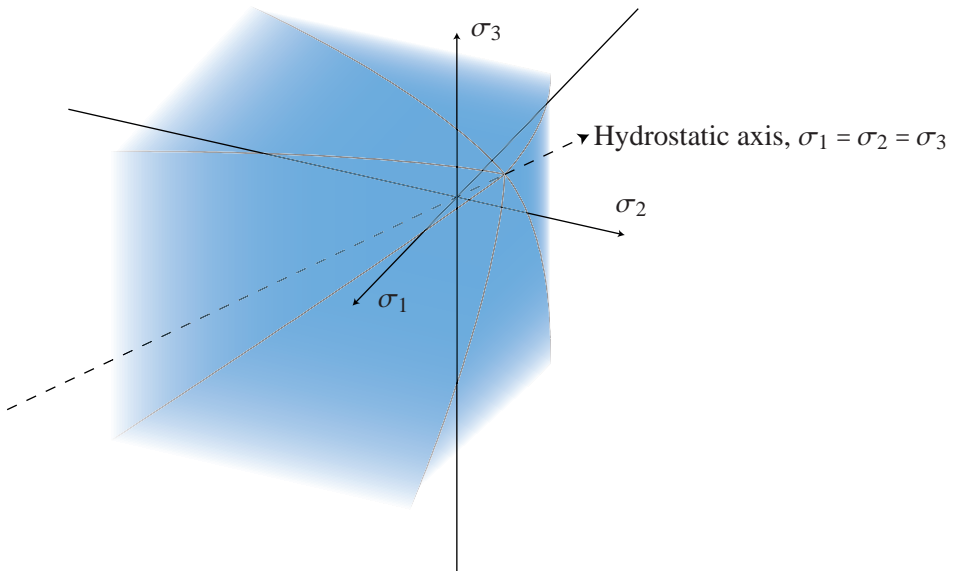


Figure 2.2: The generalized Hoek-Brown criterion visualized in principal stress space.

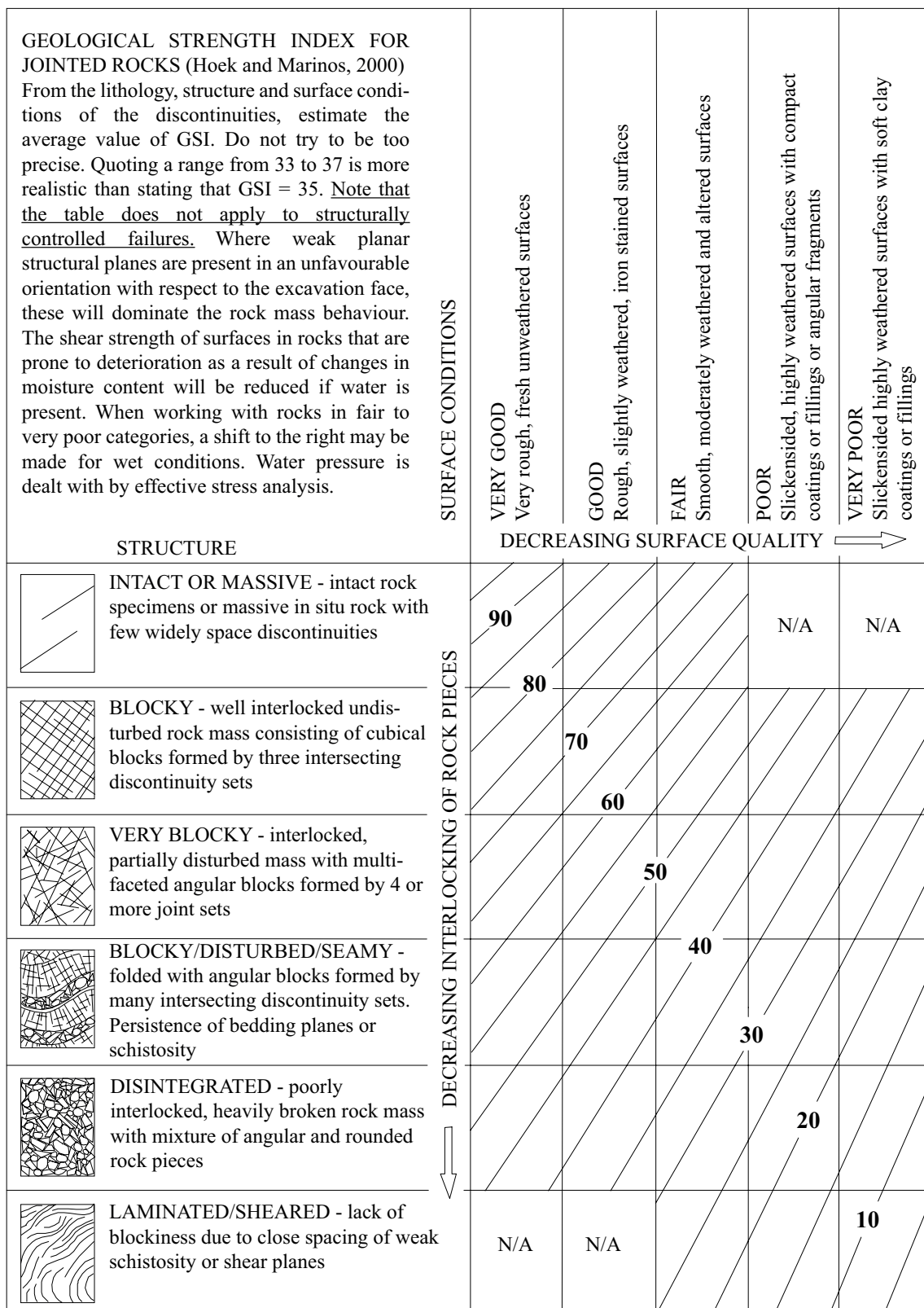


Figure 2.3: Geological strength index for jointed rock masses [Marinos and Hoek, 2000].

## The Mohr-Coulomb Criterion

Even though the Hoek-Brown criterion is specifically developed with rock materials in mind, a lot of the finite element models made today still utilize the much older Mohr-Coulomb failure criterion, which states, that once the shear stress,  $\tau$ , and the normal stress,  $\sigma_n$ , is reached in a plane in a continuum, which satisfies

$$\tau = c - \sigma_n \tan(\varphi) \quad (3.1)$$

yielding occurs.  $c$  is a measure of the cohesion present in the material, while  $\tan(\varphi)$  is a measure of the friction coefficient between the grains, thus  $\varphi$  is denoted the friction angle. In the above expression, tension is taken as positive. This linear relationship can be visualized as shown in Figure 3.1.

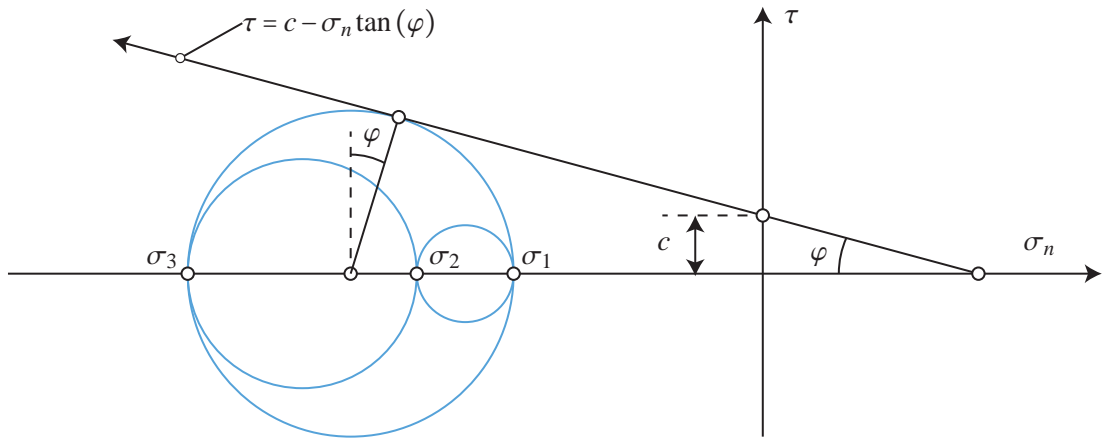


Figure 3.1: The Mohr-Coulomb criterion in  $\sigma_n$ - $\tau$  space.

Any Mohr circle situated below the Mohr-Coulomb line denotes an elastic state, whereas a Mohr circle, which touches the line denotes a state of yielding. From Figure 3.1, the shear stress causing failure can be shown to be

$$\tau = \frac{\sigma_1 - \sigma_3}{2} \cos(\varphi) \quad (3.2)$$

where  $\sigma_1$  and  $\sigma_3$  are respectively the largest and smallest principal stresses. Similarly, the normal stress on the failure plane is given by

$$\sigma_n = \frac{\sigma_1 + \sigma_3}{2} + \frac{\sigma_1 - \sigma_3}{2} \sin(\varphi) \quad (3.3)$$

Substitution back into (3.1) and rewriting results in

$$\sigma_1 - \sigma_3 + (\sigma_1 + \sigma_3) \sin(\varphi) = 2c \cos(\varphi) \quad (3.4)$$

If the implicit function above is plotted in principal stress space, it is forming a six-sided pyramid along the hydrostatic axis as shown on Figure 3.2. This shape represents the yield surface, and it is evident from the figure, that the criterion is pressure dependent. Any stress state situated inside the stress space bounded by the six planes is elastic, while stress states outside are non-allowable.

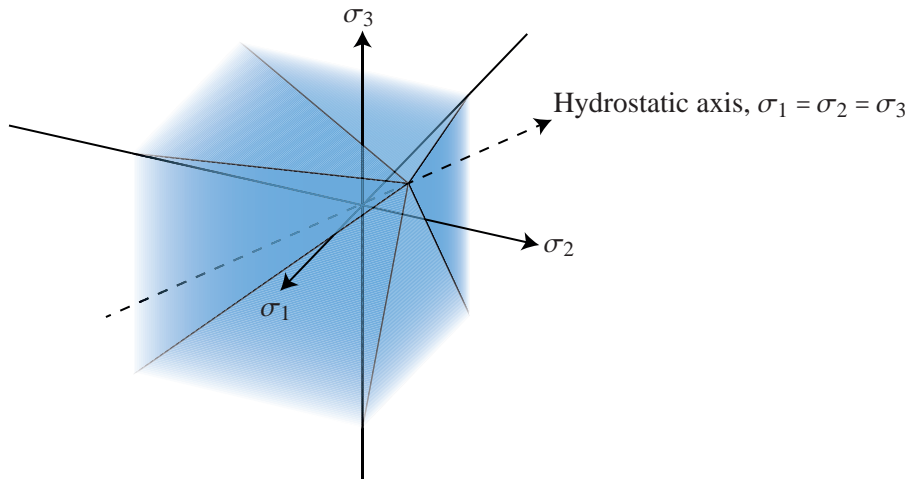


Figure 3.2: The Mohr-Coulomb criterion plotted in principal stress space.

Written as a yield function, the Mohr-Coulomb criterion takes the following formulation

$$f(\boldsymbol{\sigma}, c, \varphi) = \sigma_1 - \sigma_3 + (\sigma_1 + \sigma_3) \sin(\varphi) - 2c \cos(\varphi) = 0 \quad (3.5)$$

which can be refined to give

$$f(\boldsymbol{\sigma}, \sigma_c, k) = k\sigma_1 - \sigma_3 - \sigma_c = 0 \quad (3.6)$$

where  $k$  is given by

$$k = \frac{1 + \sin(\varphi)}{1 - \sin(\varphi)} \quad (3.7)$$

and the uniaxial compressive strength,  $\sigma_c$ , is given by

$$\sigma_c = 2c \sqrt{k} \quad (3.8)$$

### 3.1 Mohr-Coulomb Approximation of Hoek-Brown criterion

In order to use the Mohr-Coulomb criterion to model rock materials, a method of relating the Mohr-Coulomb parameters to the rock properties obtained using the Hoek-Brown criterion needs to be identified. According to Hoek et al. [2002] the friction angle can be calculated using

$$\varphi = \sin^{-1} \left( \frac{6am_b(s + m_b\sigma_{3n})^{a-1}}{2(1+a)(2+a) + 6am_b(s + m_b\sigma_{3n})^{a-1}} \right) \quad (3.9)$$

and the corresponding cohesion is given by

$$c = \frac{\sigma_{ci}((1+2a)s + (1-a)m_b\sigma_{3n})(s+m_b\sigma_{3n})^{a-1}}{(1+a)(2+a)\sqrt{1+(6am_b(s+m_b\sigma_{3n})^{a-1})/((1+a)(2+a))}} \quad (3.10)$$

where  $\sigma_{3n}$  is given by

$$\sigma_{3n} = \frac{\sigma_{3,max}}{\sigma_{ci}} \quad (3.11)$$

and  $\sigma_{3,max}$  is the upper bound over which the Mohr-Coulomb criterion is sought fitted, cf. Figure 3.3. Notice that compression is taken as positive in these derivations.

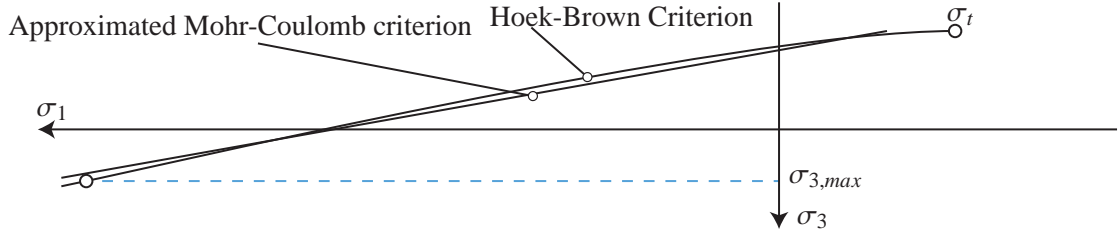


Figure 3.3: *Mohr-Coulomb approximation of Hoek-Brown criterion. Compression is taken as positive.*

The upper boundary of the stress range should be chosen based on the problem at hand, such that it covers the stress range of the model. For deep tunnels, the following relationship gives a good estimate [Hoek et al., 2002]

$$\frac{\sigma_{3,max}}{\sigma_{cm}} = 0.47 \left( \frac{\sigma_{cm}}{\gamma H} \right)^{-0.94} \quad (3.12)$$

where

$$\sigma_{cm} = \sigma_{ci} \frac{(m_b + 4s - a(m_b - 8s)) \left(\frac{m_b}{4} + s\right)^{a-1}}{2(1+a)(2+a)} \quad (3.13)$$

and  $\gamma$  is the unit weight of the rock mass, and  $H$  is the depth of the tunnel below the surface. For slope stability, the following gives a good estimate of  $\sigma_{3,max}$

$$\frac{\sigma_{3,max}}{\sigma_{cm}} = 0.72 \left( \frac{\sigma_{cm}}{\gamma H} \right)^{-0.91} \quad (3.14)$$

A more general approach is to define  $\sigma_{3,max}$  as [Rocscience Inc., 2007]

$$\sigma_{3,max} = \frac{\sigma_{ci}}{4} \quad (3.15)$$



# Plasticity Fundamentals

In this chapter, some of the basics of material plasticity is outlined. However, a detailed description is beyond the scope of this report. For a more thorough exposition, see de Souza Neto et al. [2008], Ottosen and Ristinmaa [2005] and Crisfield [2000].

## 4.1 The Yield Function

The strains that develop within a material when exposed to a load can basically be divided into two separate parts. Part of the strains are what is known as elastic strains. These strains are characterized by the fact that once the external load disappears, so does the elastic strains that developed during loading. The part of the strains which are not elastic are known as plastic. These strains remain even after the material has been unloaded. See Figure 4.1.

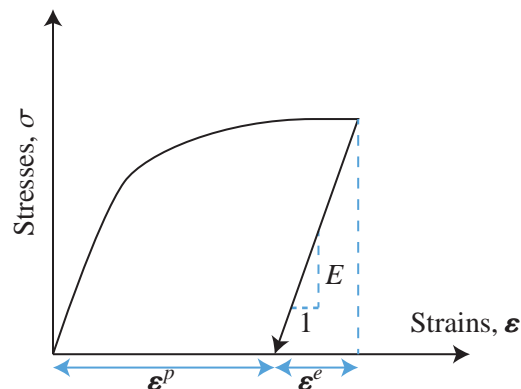


Figure 4.1: Elastic and plastic strains.

So the total strains,  $\boldsymbol{\epsilon}$ , are made up of elastic strains and plastic strains, which can be written as

$$\boldsymbol{\epsilon} = \boldsymbol{\epsilon}^e + \boldsymbol{\epsilon}^p \quad (4.1)$$

where  $\boldsymbol{\epsilon}^e$  is the elastic strain vector and  $\boldsymbol{\epsilon}^p$  is the plastic strain vector. Plastic strains start to develop once the material reaches its yielding limit, which is defined by some yield function  $f = 0$ . This could, for example, be the Hoek-Brown criterion or the Mohr-Coulomb criterion discussed earlier. The yield

function,  $f$ , is a function of the stresses as well as some hardening parameters,  $\mathbf{K}$ , which describe the strength of the material, i.e.

$$f = f(\boldsymbol{\sigma}, \mathbf{K}) \quad (4.2)$$

Sometimes, a material might require more than one yield function in order to be modeled sufficiently accurate, this is discussed in section 4.7. The hardening parameters are usually determined by some state parameters,  $\kappa$ , that determine the internal state of the material

$$\mathbf{K} = \mathbf{K}(\kappa) \quad (4.3)$$

The yield function is a scalar valued function, which gives a negative value for all stress states that are elastic. Once the yield function reaches a value of zero, plastic strains start to develop. The stress states which fulfill this criterion form a surface in stress space known as the yield surface, see e.g. Figure 2.2 and 3.2. Further, the yield function remains zero during plastic loading, which implies that the time derivative of  $f$  during plastic loading is zero, which can be written as

$$\frac{df}{dt} = \frac{\partial f}{\partial t} \frac{dt}{dt} + \left( \frac{\partial f}{\partial \boldsymbol{\sigma}} \right)^T \frac{d\boldsymbol{\sigma}}{dt} + \left( \frac{\partial f}{\partial \mathbf{K}} \right)^T \frac{\partial \mathbf{K}}{\partial \kappa} \frac{d\kappa}{dt} = 0 \quad (4.4)$$

which is known as the consistency relation. Since the yield function is time-independent, it simplifies to

$$\frac{df}{dt} = \mathbf{a}^T \frac{d\boldsymbol{\sigma}}{dt} + \left( \frac{\partial f}{\partial \mathbf{K}} \right)^T \frac{\partial \mathbf{K}}{\partial \kappa} \frac{d\kappa}{dt} = 0 \quad (4.5)$$

where  $\mathbf{a}$  is given by

$$\mathbf{a} = \frac{\partial f}{\partial \boldsymbol{\sigma}} \quad (4.6)$$

The time-dependency is discussed further in section 4.5. A stress state which returns a positive value of the yield function is inadmissible. The stress state within the material is determined by the elastic strains through the constitutive matrix,  $\mathbf{D}$ , as

$$\boldsymbol{\sigma} = \mathbf{D}\boldsymbol{\epsilon}^e = \mathbf{D}(\boldsymbol{\epsilon} - \boldsymbol{\epsilon}^p) \quad (4.7)$$

where (4.1) has been used. If no plastic straining has occurred in the material, the relationship between stresses and strains is one-to-one. I.e. it is possible to determine the stress state based on the total strains, which merely consist of elastic strains. However, if plastic straining has developed within the material, the one-to-one relationship is lost, see Figure 4.2. The stress state is said to be path-dependent.

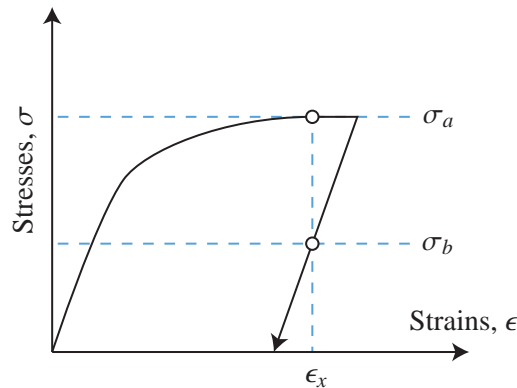


Figure 4.2: The one-to-one relationship between strains and stresses are lost once plastic strains have developed.

Because of this path-dependence, it is necessary to adopt an incremental approach in order to find matching strain-stress relations. This is done by taking the time derivative of (4.7), which can be written as

$$\frac{d\sigma}{dt} = \mathbf{D} \frac{d\epsilon}{dt} = \mathbf{D} \left( \frac{d\epsilon}{dt} - \frac{d\epsilon^p}{dt} \right) \quad (4.8)$$

## 4.2 Plastic Potential

Once the yield function reaches zero and plastic strains start to develop, it is crucial to know in which direction they develop. However there is no conclusive way to determine this. A way to get around this, is to define a plastic potential function,  $g$ . The plastic potential is a scalar valued function, which usually depends upon the stress state and some hardening parameters

$$g = g(\boldsymbol{\sigma}, \mathbf{K}) \quad (4.9)$$

The partial derivative of this plastic potential with respect to the stresses define the direction of the plastic strains. A common choice for the plastic potential is to use the yield function. If this is the case, it is referred to as associated plasticity. If another function is chosen, it is referred to as non-associated plasticity. The length of the incremental plastic strain is controlled by a so called plastic multiplier,  $d\lambda$ , which is a non-negative scalar. Thus the plastic strain increment is given by

$$\frac{d\epsilon^p}{dt} = \frac{d\lambda}{dt} \frac{\partial g}{\partial \sigma} = \frac{d\lambda}{dt} \mathbf{b} \quad (4.10)$$

where the abbreviation  $\mathbf{b}$  has been introduced to improve readability. This relation is known as the flow rule.

## 4.3 Hardening and Softening

As mentioned earlier, rock material tend to lose some of its strength once plastic straining occurs, which is known as softening. However many metals tend to show an increase in strength during plastic straining, see Figure 1.1a, which is known as hardening. Usually both phenomena are simply referred to as hardening. If the material is considered perfectly plastic, the yield criterion is independent of the hardening parameters  $\mathbf{K}$ , and simply reduces to

$$f(\boldsymbol{\sigma}, \mathbf{K}) = f(\boldsymbol{\sigma}) = F(\boldsymbol{\sigma}) = 0 \quad (4.11)$$

where  $F$  has been introduced for readability and designates a perfectly plastic yield function. If hardening is employed in the model, two distinct methods are normally chosen, namely the isotropic hardening model and the kinematic hardening model, see Figure 4.3. The isotropic hardening model expands or contracts the yield surface, which can be achieved by adding or subtracting an appropriate amount from the yield criterion based upon the state variables  $\mathbf{k}$ . However, the position and shape of the yield surface in stress space is unaltered. This can be expressed as

$$f(\boldsymbol{\sigma}, \mathbf{K}) = F(\boldsymbol{\sigma}) - \mathbf{K} = 0 \quad (4.12)$$

On the other hand, kinematic hardening shifts the yield surface from one location in stress space to another. The size and shape of the yield surface remains unaltered. This can be achieved by shifting the

stresses by some amount defined by the state variables as

$$f(\boldsymbol{\sigma}, \mathbf{K}) = F(\boldsymbol{\sigma} - \mathbf{K}) = 0 \quad (4.13)$$

The two different hardening models can be used simultaneously, in which case it is referred to as mixed hardening. Mixed hardening alters the size and position of the yield surface and leaves the shape unaltered. This can be written as

$$f(\boldsymbol{\sigma}, \mathbf{K}) = F(\boldsymbol{\sigma} - \mathbf{K}_{kin}) - \mathbf{K}_{iso} = 0 \quad (4.14)$$

where  $\mathbf{K}_{kin}$  and  $\mathbf{K}_{iso}$  are the hardening parameters associated with kinematic hardening and isotropic hardening respectively.

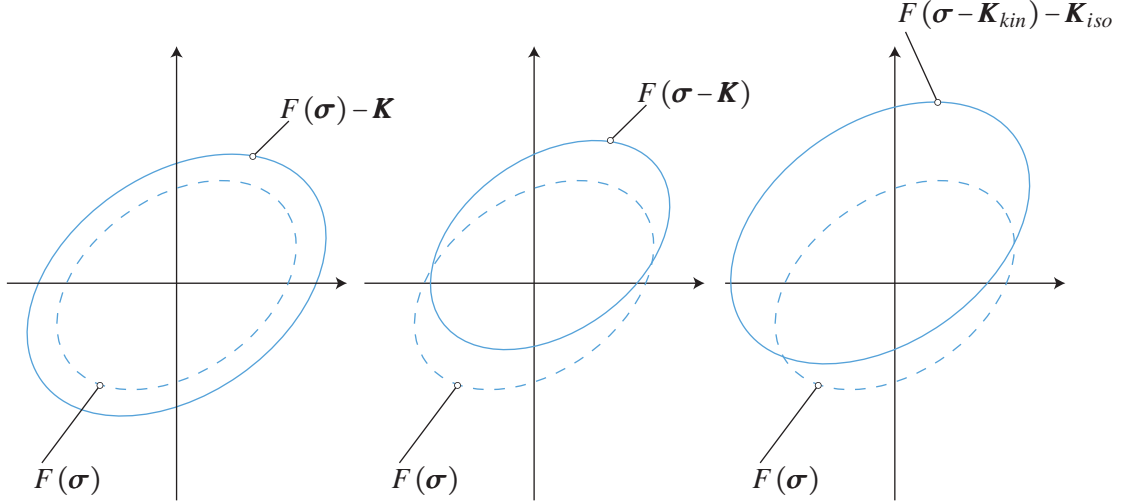


Figure 4.3: Isotropic, kinematic and mixed hardening.

## 4.4 State Parameters

The state parameters which control the hardening of the material need to be identified and their time rate of change has to be established, the so-called evolution law. The two most common state parameters are the accumulated plastic strain, denoted,  $\bar{\epsilon}^p$ , and the dissipated plastic work,  $W^p$ , defined by

$$W^p = \int_0^{\bar{\epsilon}^p} \boldsymbol{\sigma}^T d\boldsymbol{\epsilon}^p \quad (4.15)$$

The accumulated plastic strain can be defined in different manners, in which the most common is the Von Mises accumulated plastic strain defined by

$$\bar{\epsilon}^p = \sqrt{\frac{2}{3} \left( \frac{d\boldsymbol{\epsilon}^p}{dt} \right)^T \frac{d\boldsymbol{\epsilon}^p}{dt}} dt \quad (4.16)$$

Alternatively, the state parameters can also be defined by some potential function,  $j$ , which is a function of the stress state and the hardening variables

$$j = j(\boldsymbol{\sigma}, \mathbf{K}) \quad (4.17)$$

and a plastic multiplier, using the following expression

$$\frac{d\kappa}{dt} = -\frac{d\lambda}{dt} \frac{\partial j}{\partial \mathbf{K}} \quad (4.18)$$

For instance, if the state parameter is the accumulated plastic strain,  $\bar{\epsilon}^p$ , and the hardening parameter is the cohesion,  $c$ , the increment of the accumulated plastic strain is given as

$$\frac{d\bar{\epsilon}^p}{dt} = -\frac{d\lambda}{dt} \frac{\partial j}{\partial c} \quad (4.19)$$

If  $j$  is assumed equal to  $f$ , the evolution law is said to be associated, and if  $j$  is different from  $f$ , the evolution law is said to be non-associated.

## 4.5 Time-Independency

As can be seen from the above equations, there are a lot of first order time derivatives, which represent the load rate of the problem. If a solution is sought, which is independent of the load rate, these time rate of changes can simply be thought of as changes in the variables which are being differentiated. For example, the time rate of change of the plastic strains

$$\frac{d\boldsymbol{\epsilon}^p}{dt} \quad (4.20)$$

can be replaced with

$$d\boldsymbol{\epsilon}^p \quad (4.21)$$

and thought of as a nothing more than an infinitesimal change in the plastic strains, regardless of time. By adopting this independency, the consistency relation, equation (4.5), can be written as

$$df = \mathbf{a}^T d\boldsymbol{\sigma} + \left( \frac{\partial f}{\partial \mathbf{K}} \right)^T \frac{\partial \mathbf{K}}{\partial \kappa} d\kappa = 0 \quad (4.22)$$

The stress increment, equation (4.8), can be written as

$$d\boldsymbol{\sigma} = \mathbf{D} (d\boldsymbol{\epsilon} - d\boldsymbol{\epsilon}^p) \quad (4.23)$$

The flow rule, equation (4.10), can be written as

$$d\boldsymbol{\epsilon}^p = d\lambda \mathbf{b} \quad (4.24)$$

and finally, the evolution law defined by a potential function, equation (4.18), can be written as

$$d\kappa = -d\lambda \frac{\partial j}{\partial \mathbf{K}} \quad (4.25)$$

## 4.6 Infinitesimal Constitutive Matrix

The infinitesimal constitutive matrix,  $\mathbf{D}^{ep}$ , relates infinitesimal strain increments with infinitesimal stress increments as follows

$$d\boldsymbol{\sigma} = \mathbf{D}^{ep} d\boldsymbol{\epsilon} \quad (4.26)$$

Combining the consistency relation, equation (4.22), the infinitesimal stress increment, equation (4.23), the plastic flow rule, equation (4.24), and the evolution law, a solution for the infinitesimal increment of the plastic multiplier,  $d\lambda$ , can be found. If the hardening law is assumed to be defined by a potential function,  $j$ , as in equation (4.25),  $d\lambda$  is found to be

$$d\lambda = \frac{\mathbf{a}^T \mathbf{D} d\boldsymbol{\epsilon}}{\mathbf{a}^T \mathbf{D} \mathbf{b} + \left( \frac{\partial f}{\partial \mathbf{K}} \right)^T \frac{\partial \mathbf{K}}{\partial \boldsymbol{\kappa}} \frac{\partial j}{\partial \mathbf{K}}} \quad (4.27)$$

If this solution is substituted back into equation (4.23), the infinitesimal constitutive matrix can be found to be

$$\mathbf{D}^{ep} = \mathbf{D} - \frac{\mathbf{D} \mathbf{b} \mathbf{a}^T \mathbf{D}}{\mathbf{a}^T \mathbf{D} \mathbf{b} + \left( \frac{\partial f}{\partial \mathbf{K}} \right)^T \frac{\partial \mathbf{K}}{\partial \boldsymbol{\kappa}} \frac{\partial j}{\partial \mathbf{K}}} \quad (4.28)$$

## 4.7 Multiple Yield Functions

Some yield criteria might consist of multiple yield functions

$$f_1(\boldsymbol{\sigma}, \mathbf{K}), f_2(\boldsymbol{\sigma}, \mathbf{K}), \dots, f_n(\boldsymbol{\sigma}, \mathbf{K}) \quad (4.29)$$

Each yield function defines a surface in stress space. In this case, the elastic stress states are bounded by the stress states which return a negative value of all the yield functions. See Figure 4.4

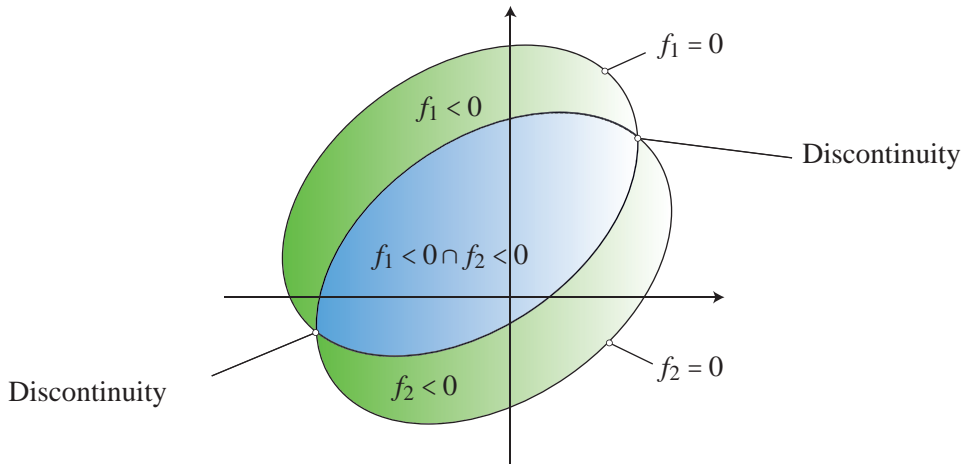


Figure 4.4: The elastic stress states (blue) of a yield criterion with multiple yield functions (green).

In these cases, the combined yield surface contains intersections between the individual yield functions, which require special attention. These intersections can be visualized as curves and points in principal stress space and is known as yield curves and yield points, see e.g. Figure 2.2 and Figure 3.2. These intersections usually result in discontinuities where the surfaces of the yield functions intersect, see Figure 4.4. If multiple yield functions are utilized, each yield function typically have a unique plastic potential,  $g_i$ , and hardening potential,  $j_i$ . In such cases, the strain direction at a discontinuous part of a yield criterion, see Figure 4.5, is a linear combination of the different strain directions involved

[Koiter, 1953]

$$d\boldsymbol{\varepsilon}^p = \sum_{i=1}^k d\lambda_i \mathbf{b}_i \quad (4.30)$$

where  $k$  is the number of plastic potentials, that is part of the intersection at hand. Similarly, the evolution law is given by

$$d\boldsymbol{\kappa} = - \sum_{i=1}^k d\lambda_i \frac{\partial j_i}{\partial \mathbf{K}} \quad (4.31)$$

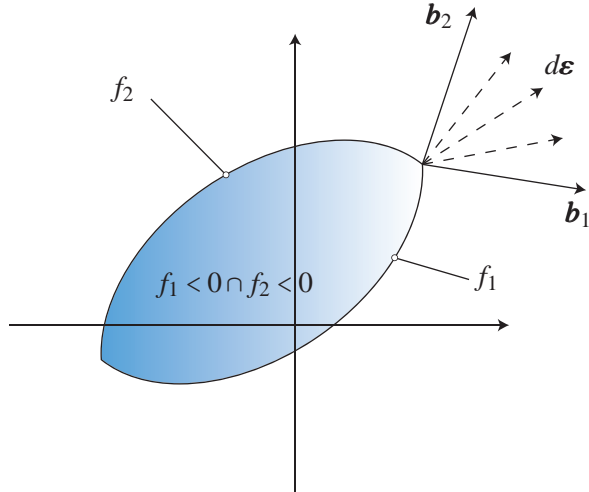


Figure 4.5: The plastic strain direction at a discontinuous part of the yield criteria.



---

# Return Mapping in General Stress Space

In this chapter, the theory behind return mapping is introduced. However, a short introduction to the non-linear finite element method is given first, in order show the need and applicability of return mapping. For a more detailed description of the theory behind return mapping and finite element methods, see de Souza Neto et al. [2008], Cook et al. [2002] and Crisfield [2000]. The derivations of this chapter rely on a evolution law of the form given by equation (4.25) and (4.31).

## 5.1 Non-linear Finite Element Method

Problems involving the displacement and stress distribution throughout a model can be formulated as partial differential equations made up of the governing equations behind the problem and some boundary conditions, which make the model unique. However, for complex models, an analytical solution to these boundary value problems is very hard or simply impossible to establish. Because of this, the problem is sought solved through numerical integration, which is where the finite element method comes into play.

As the name suggests, the model is discretized into a finite number of elements, for which the solution to the governing equations can be approximated with polynomials. A large range of different elements exist, each with advantages and disadvantages, however this is beyond the scope of this report. Based on this discretization, the stiffness of the entire model can be calculated. Because the stiffness of the model is non-linear and path dependent, the boundary conditions are applied incrementally in what is known as load steps. The system of equations is solved iteratively in each load step, to make sure that equilibrium is fulfilled. Usually by the use of a Newton-Raphson scheme. This process can be schematized as shown in Table 5.1. The highlighted points of the procedure are material dependent and is the main focus of this report. The updated stress state should ideally be found through and integration of the infinitesimal elasto-plastic constitutive matrix along the path of the strain increment as

$$\boldsymbol{\sigma}_k = \boldsymbol{\sigma}_{k-1} + \int_{\boldsymbol{\epsilon}_{k-1}}^{\boldsymbol{\epsilon}_{k-1} + \Delta\boldsymbol{\epsilon}} d\boldsymbol{\sigma} = \boldsymbol{\sigma}_{k-1} + \int_{\boldsymbol{\epsilon}_{k-1}}^{\boldsymbol{\epsilon}_{k-1} + \Delta\boldsymbol{\epsilon}} \mathbf{D}^{ep} d\boldsymbol{\epsilon} \quad (5.1)$$

where equation (4.26) has been used. However, the integration of equation (5.1) is no easy task, since the strain path is unknown and  $\mathbf{D}^{ep}$  is stress dependent. Several methods exist, which try to circumvent this problem. Return mapping is one of these methods, and is the method used throughout this report.

<ul style="list-style-type: none"> <li>Q Load step <math>k = 1, 2, \dots</math></li> <li>o <math>\mathbf{p}_k = \mathbf{p}_{k-1} + \Delta\mathbf{p}_k</math></li> <li>o <math>\Delta\mathbf{u}_1 = \mathbf{0}</math></li> <li>o <math>\boldsymbol{\sigma}_k = \boldsymbol{\sigma}_{k-1}</math></li> <li>o Q Global equilibrium iterations <math>j = 1, 2, \dots</math></li> <li>o o <math>\mathbf{r} = \mathbf{p}_k - \mathbf{q}(\boldsymbol{\sigma}_k)</math></li> <li>o o <math>\mathbf{K}(\mathbf{D}^{epc})</math></li> <li>o o <math>\delta\mathbf{u} = \mathbf{K}^{-1}\mathbf{r}</math></li> <li>o o <math>\Delta\mathbf{u}_{j+1} = \Delta\mathbf{u}_j + \delta\mathbf{u}</math></li> <li>o o <math>\Delta\boldsymbol{\epsilon} = \mathbf{B}\Delta\mathbf{u}_{j+1}</math></li> <li>o o <math>\boldsymbol{\sigma}_k(\boldsymbol{\sigma}_{k-1}, \Delta\boldsymbol{\epsilon})</math></li> <li>o o <math>\mathbf{D}^{epc}(\boldsymbol{\sigma}_k)</math></li> <li>o ● Stop iterations when <math>\ \mathbf{r}\  &lt; \epsilon\ \mathbf{p}_k\ </math></li> <li>o <math>\mathbf{u}_k = \mathbf{u}_{k-1} + \Delta\mathbf{u}_{j+1}</math></li> <li>o <math>\boldsymbol{\epsilon}_k = \mathbf{B}\mathbf{u}_k</math></li> <li>● End of load step</li> </ul>	<ul style="list-style-type: none"> <li>Initiation of the <math>k</math>th load vector</li> <li>Initiation of the displacement increment</li> <li>Initiation of start guess of <math>\boldsymbol{\sigma}_k</math></li> <li>Force residual, <math>\mathbf{r}</math>, from <math>\mathbf{p}_k</math> and internal forces, <math>\mathbf{q}</math></li> <li>Form the global tangent stiffness matrix, <math>\mathbf{K}</math></li> <li>Solve the FEM equations</li> <li>Update displacement increment</li> <li>Calculate strain increment</li> <li><b>Update stresses</b></li> <li><b>Update consistent constitutive matrix</b></li> <li><math>\epsilon</math> is a prescribed tolerance</li> <li>Update displacement vector</li> <li>Update strain vector</li> </ul>
---	---

Table 5.1: *Schematic of the incremental nature of the non-linear finite element method and the Newton-Raphson procedure used in the global equilibrium iterations. Based on [Clausen, 2007]*

Further, if the infinitesimal constitutive matrix,  $\mathbf{D}^{ep}$ , relating infinitesimal strain increments with infinitesimal stress increments, is used in the global equilibrium iteration scheme of the finite element code, where finite increments are used, the quadratic convergence of the problem will be lost [Nagtegaal, 1982]. Because of this, a consistent constitutive matrix,  $\mathbf{D}^{epc}$ , is developed, which maintains the quadratic convergence by relating infinitesimal changes of the finite strain increments with infinitesimal changes of the finite stress increments

$$d\Delta\boldsymbol{\sigma} = \mathbf{D}^{epc} d\Delta\boldsymbol{\epsilon} \quad (5.2)$$

## 5.2 Return Mapping Basics

The fundamental idea of return mapping is to try out, whether the entire strain increment,  $\Delta\boldsymbol{\epsilon}$ , is elastic by introducing the elastic predictor stress increment

$$\Delta\boldsymbol{\sigma}^e = \mathbf{D}\Delta\boldsymbol{\epsilon} \quad (5.3)$$

Adding this, to the initial stress state, see Figure 5.1,

$$\boldsymbol{\sigma}^A = \boldsymbol{\sigma}_{k-1} \quad (5.4)$$

the predicted elastic stress state,  $\boldsymbol{\sigma}^B$ , becomes

$$\boldsymbol{\sigma}^B = \boldsymbol{\sigma}^A + \Delta\boldsymbol{\sigma}^e \quad (5.5)$$

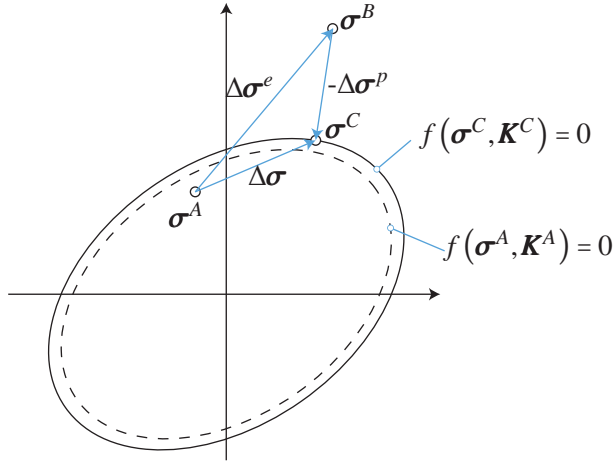


Figure 5.1: Sketch of the updating scheme.

If  $\sigma^B$  returns a negative value of the yield function, i.e.  $f(\sigma^B) \leq 0$ , the entire strain increment is purely elastic, and no further calculations are needed. However, if the predicted stress state falls outside the yield surface, a part of the strain increment must consist of plastic strains. According to equation (4.23), the stress increment must be given by

$$\Delta\sigma = \int_{\epsilon_{k-1}}^{\epsilon_{k-1} + \Delta\epsilon} D(d\epsilon - d\epsilon^p) = D\Delta\epsilon - D\Delta\epsilon^p \quad (5.6)$$

where use has been made of the fact, that  $D$  is independent of  $\epsilon$ , because linear elasticity is assumed. Introducing the plastic corrector stress increment, see Figure 5.1

$$\Delta\sigma^p = D\Delta\epsilon^p \quad (5.7)$$

together with equation (5.3), the stress increment is given by

$$\Delta\sigma = \Delta\sigma^e - \Delta\sigma^p \quad (5.8)$$

and the final updated stress state,  $\sigma^C$ , becomes

$$\sigma^C = \sigma^A + \Delta\sigma \quad (5.9)$$

which can also be written as

$$\sigma^C = \sigma^B - \Delta\sigma^p \quad (5.10)$$

Using equation (4.24), the plastic strain increment,  $\Delta\epsilon^p$ , used in calculating the plastic corrector,  $\Delta\sigma^p$ , is given by

$$\Delta\epsilon^p = \int_{\lambda}^{\lambda + \Delta\lambda} b d\lambda \quad (5.11)$$

The integration of equation (5.11) is just as complicated as equation (5.1), however, in the return mapping framework, the plastic strain increment is approximated with

$$\Delta\epsilon^p \approx \Delta\lambda b|_C \quad (5.12)$$

which results in the plastic corrector increment,  $\Delta\boldsymbol{\sigma}^P$ , can be written as

$$\Delta\boldsymbol{\sigma}^P \approx \Delta\lambda \mathbf{D} \mathbf{b}|_C \quad (5.13)$$

and thus the problem boils down to finding the updated stress state,  $\boldsymbol{\sigma}^C$ , which fulfills equation (5.10) and lies on the yield surface. If the updated stress state belongs to a single active yield function, cf. equation (4.24), the plastic corrector increment is given as shown above. However, if the updated stress state belongs to an intersection of two or more yield functions, the plastic strain direction is given by equation (4.30). Because of this, slightly different return mapping procedures have to be deployed, depending on the number of active yield functions that the updated stress state,  $\boldsymbol{\sigma}^C$ , belongs to.

### 5.3 Return to One Active Yield Function

The updated stress state,  $\boldsymbol{\sigma}^C$ , belongs to the yield surface defined by the yield function hence

$$f(\boldsymbol{\sigma}^C, \mathbf{K}^C) = 0 \quad (5.14)$$

where  $\mathbf{K}^C$  are the updated hardening variables

$$\mathbf{K}^C = \mathbf{K}(\kappa^C) \quad (5.15)$$

and  $\kappa^C$  are the updated state parameters. In case of a hardening law based upon a potential function, this could be written as follows

$$\kappa^C = \kappa^A - \Delta\lambda \left. \frac{\partial j}{\partial \mathbf{K}} \right|_C \quad (5.16)$$

In order to find the correct updated stress state and the plastic multiplier, equation (5.10) and (5.14) are solved using an iterative procedure, for instance a Newton-Raphson procedure, which is used in this text.

#### 5.3.1 Consistent Constitutive Matrix

$\mathbf{D}^{epc}$  is derived by taking the total derivative of (5.8) with respect to  $\Delta\boldsymbol{\epsilon}$ , using (5.3) and (5.13) as follows

$$\frac{d\Delta\boldsymbol{\sigma}}{d\Delta\boldsymbol{\epsilon}} = \frac{d\mathbf{D}\Delta\boldsymbol{\epsilon}}{d\Delta\boldsymbol{\epsilon}} - \frac{\partial\Delta\lambda\mathbf{D}\mathbf{b}}{\partial\Delta\lambda} \cdot \frac{d\Delta\lambda}{d\Delta\boldsymbol{\epsilon}} - \frac{\partial\Delta\lambda\mathbf{D}\mathbf{b}}{\partial\Delta\boldsymbol{\sigma}} \cdot \frac{d\Delta\boldsymbol{\sigma}}{d\Delta\boldsymbol{\epsilon}} \quad (5.17)$$

Multiplying with  $d\Delta\boldsymbol{\epsilon}$  on both sides yields

$$d\Delta\boldsymbol{\sigma} = \mathbf{D} d\Delta\boldsymbol{\epsilon} - \mathbf{D}\mathbf{b} d\Delta\lambda - \Delta\lambda \mathbf{D} \frac{\partial\mathbf{b}}{\partial\boldsymbol{\sigma}} d\Delta\boldsymbol{\sigma} \quad (5.18)$$

Rearranging leads to

$$d\Delta\boldsymbol{\sigma} = \left( \mathbf{I} + \Delta\lambda \mathbf{D} \frac{\partial\mathbf{b}}{\partial\boldsymbol{\sigma}} \right)^{-1} \mathbf{D} (d\Delta\boldsymbol{\epsilon} - d\Delta\lambda\mathbf{b}) \quad (5.19)$$

which can be written on the form

$$d\Delta\boldsymbol{\sigma} = \mathbf{D}^c d\Delta\boldsymbol{\epsilon} - d\Delta\lambda \mathbf{D}^c \mathbf{b} \quad (5.20)$$

where

$$\mathbf{D}^c = \mathbf{T} \mathbf{D} \quad (5.21)$$

$$\mathbf{T} = \left( \mathbf{I} + \Delta\lambda \mathbf{D} \frac{\partial\mathbf{b}}{\partial\boldsymbol{\sigma}} \right)^{-1} \quad (5.22)$$

$\mathbf{D}$  is known as the modification matrix. Using the consistency condition, (4.22), an expression for  $d\Delta\lambda$  can be found in much the same way as it was found in (4.27), and substituted back into (5.20), which gives the consistent constitutive matrix as

$$\mathbf{D}^{epc} = \mathbf{D}^c - \frac{\mathbf{D}^c \mathbf{b} \mathbf{a}^T \mathbf{D}^c}{\mathbf{a}^T \mathbf{D}^c \mathbf{b} + \left( \frac{\partial f}{\partial \mathbf{K}} \right)^T \frac{\partial \mathbf{K}}{\partial \mathbf{K}} \frac{\partial j}{\partial \mathbf{K}}} \quad (5.23)$$

If  $\mathbf{a}$  is equal to  $\mathbf{b}$ , it is seen, that  $\mathbf{D}^{epc}$  is symmetric.

## 5.4 Return to Two Active Yield Functions

If the yield criterion consists of two yield functions,  $f_1$  and  $f_2$ , with the appertaining plastic potentials  $g_1$  and  $g_2$  and the hardening potentials  $j_1$  and  $j_2$ , it is possible, that the updated stress state belongs to the intersection of these two yield surfaces, see Figure 4.4. If this is the case, the direction of the plastic strains is given by equation (4.30), and thus the corrector stress is also a linear combination of the stress directions involved giving

$$\Delta\boldsymbol{\sigma}^p = \Delta\lambda_1 \mathbf{D} \mathbf{b}_1|_C + \Delta\lambda_2 \mathbf{D} \mathbf{b}_2|_C \quad (5.24)$$

where

$$\mathbf{b}_1 = \frac{\partial g_1}{\partial \boldsymbol{\sigma}} \quad (5.25)$$

$$\mathbf{b}_2 = \frac{\partial g_2}{\partial \boldsymbol{\sigma}} \quad (5.26)$$

$$(5.27)$$

Similarly, the hardening law, equation (5.16) expands to

$$\boldsymbol{\kappa}^C = \boldsymbol{\kappa}^A - \Delta\lambda_1 \left. \frac{\partial j_1}{\partial \mathbf{K}} \right|_C - \Delta\lambda_2 \left. \frac{\partial j_2}{\partial \mathbf{K}} \right|_C \quad (5.28)$$

when using the hardening potential method. The updated stress state belonging to the yield curve still needs to fulfill (5.10) as well as  $f_1(\boldsymbol{\sigma}^C, \mathbf{K}^C) = 0$  and  $f_2(\boldsymbol{\sigma}^C, \mathbf{K}^C) = 0$ . This results in eight equations with eight unknowns, namely  $\boldsymbol{\sigma}^C$ ,  $\Delta\lambda_1$  and  $\Delta\lambda_2$ . To find the updated stress state,  $\boldsymbol{\sigma}^C$ , an iterative procedure is implemented in which the residual,  $\mathbf{r}$ , of equation (5.10) is defined by

$$\mathbf{r}(\boldsymbol{\sigma}^C, \Delta\lambda_1, \Delta\lambda_2) = \boldsymbol{\sigma}^C - (\boldsymbol{\sigma}^B - \Delta\lambda_1 \mathbf{D} \mathbf{b}_1|_C - \Delta\lambda_2 \mathbf{D} \mathbf{b}_2|_C) = \mathbf{0} \quad (5.29)$$

Expanding  $\mathbf{r}$  in a first order Taylor series leads to

$$\begin{aligned} \mathbf{r}(\boldsymbol{\sigma}_{i+1}^C, \Delta\lambda_{1,i+1}, \Delta\lambda_{2,i+1}) &= \mathbf{r}(\boldsymbol{\sigma}_i^C + d\boldsymbol{\sigma}, \Delta\lambda_{1,i} + d\Delta\lambda_1, \Delta\lambda_{2,i} + d\Delta\lambda_2) \\ &= \mathbf{r}(\boldsymbol{\sigma}_i^C, \Delta\lambda_{1,i}, \Delta\lambda_{2,i}) + \frac{\partial \mathbf{r}}{\partial \boldsymbol{\sigma}} d\boldsymbol{\sigma} + \frac{\partial \mathbf{r}}{\partial \Delta\lambda_1} d\Delta\lambda_1 + \frac{\partial \mathbf{r}}{\partial \Delta\lambda_2} d\Delta\lambda_2 \end{aligned} \quad (5.30)$$

where

$$\frac{\partial \mathbf{r}}{\partial \boldsymbol{\sigma}} = \frac{\partial \boldsymbol{\sigma}^C}{\partial \boldsymbol{\sigma}} - \frac{\partial \boldsymbol{\sigma}^B}{\partial \boldsymbol{\sigma}} + \frac{\partial \Delta\lambda_1 \mathbf{D} \mathbf{b}_1}{\partial \boldsymbol{\sigma}} + \frac{\partial \Delta\lambda_2 \mathbf{D} \mathbf{b}_2}{\partial \boldsymbol{\sigma}} \quad (5.31)$$

$$= \mathbf{I} + \Delta\lambda_1 \mathbf{D} \frac{\partial \mathbf{b}_1}{\partial \boldsymbol{\sigma}} + \Delta\lambda_2 \mathbf{D} \frac{\partial \mathbf{b}_2}{\partial \boldsymbol{\sigma}} \quad (5.32)$$

and

$$\frac{\partial \mathbf{r}}{\partial \Delta \lambda_1} = \mathbf{D}\mathbf{b}_1 \quad (5.33)$$

$$\frac{\partial \mathbf{r}}{\partial \Delta \lambda_2} = \mathbf{D}\mathbf{b}_2 \quad (5.34)$$

substituting back into (5.30) yields

$$\begin{aligned} \mathbf{r}(\boldsymbol{\sigma}_{i+1}^C, \Delta \lambda_{1,i+1}, \Delta \lambda_{2,i+1}) &= \mathbf{r}(\boldsymbol{\sigma}_i^C, \Delta \lambda_{1,i}, \Delta \lambda_{2,i}) + \left( \mathbf{I} + \Delta \lambda_1 \mathbf{D} \frac{\partial \mathbf{b}_1}{\partial \boldsymbol{\sigma}} + \Delta \lambda_2 \mathbf{D} \frac{\partial \mathbf{b}_2}{\partial \boldsymbol{\sigma}} \right) d\boldsymbol{\sigma} + \\ &\quad + \mathbf{D}\mathbf{b}_1 \cdot d\Delta \lambda_1 + \mathbf{D}\mathbf{b}_2 \cdot d\Delta \lambda_2 \end{aligned} \quad (5.35)$$

and solving for  $\mathbf{r}(\boldsymbol{\sigma}_{i+1}^C, \Delta \lambda_{1,i+1}, \Delta \lambda_{2,i+1}) = 0$  gives

$$\begin{aligned} d\boldsymbol{\sigma} &= \left( \mathbf{I} + \Delta \lambda_1 \mathbf{D} \frac{\partial \mathbf{b}_1}{\partial \boldsymbol{\sigma}} + \Delta \lambda_2 \mathbf{D} \frac{\partial \mathbf{b}_2}{\partial \boldsymbol{\sigma}} \right)^{-1} (-\mathbf{r}(\boldsymbol{\sigma}_i^C, \Delta \lambda_{1,i}, \Delta \lambda_{2,i}) - \mathbf{D}\mathbf{b}_1 d\Delta \lambda_2 - \mathbf{D}\mathbf{b}_2 d\Delta \lambda_2) \\ &= -\mathbf{T}\mathbf{r}(\boldsymbol{\sigma}_i^C, \Delta \lambda_{1,i}, \Delta \lambda_{2,i}) - \mathbf{D}^c \mathbf{b}_1 d\Delta \lambda_2 - \mathbf{D}^c \mathbf{b}_2 d\Delta \lambda_2 \end{aligned} \quad (5.36)$$

where

$$\mathbf{T} = \left( \mathbf{I} + \Delta \lambda_1 \mathbf{D} \frac{\partial \mathbf{b}_1}{\partial \boldsymbol{\sigma}} + \Delta \lambda_2 \mathbf{D} \frac{\partial \mathbf{b}_2}{\partial \boldsymbol{\sigma}} \right)^{-1} \quad (5.37)$$

Having an initial guess of  $\boldsymbol{\sigma}_i^C$ ,  $\Delta \lambda_{1,i}$  and  $\Delta \lambda_{2,i}$ , a Taylor expansion of the two yield criteria results in

$$\begin{aligned} f_1(\boldsymbol{\sigma}_{i+1}^C, \mathbf{K}_{i+1}^C) &= f_1(\boldsymbol{\sigma}_i^C + d\boldsymbol{\sigma}, \mathbf{K}_i^C + d\mathbf{K}) \\ &= f_1(\boldsymbol{\sigma}_i^C, \mathbf{K}_i^C) + \mathbf{a}_1^T d\boldsymbol{\sigma} + \left( \frac{\partial f_1}{\partial \mathbf{K}} \right)^T d\mathbf{K} \end{aligned} \quad (5.38)$$

where

$$\begin{aligned} d\mathbf{K} &= \frac{\partial \mathbf{K}}{\partial \boldsymbol{\kappa}} \frac{\partial \boldsymbol{\kappa}}{\partial \Delta \lambda_1} d\Delta \lambda_1 + \frac{\partial \mathbf{K}}{\partial \boldsymbol{\kappa}} \frac{\partial \boldsymbol{\kappa}}{\partial \Delta \lambda_2} d\Delta \lambda_2 \\ &= -\frac{\partial \mathbf{K}}{\partial \boldsymbol{\kappa}} \frac{\partial j_1}{\partial \mathbf{K}} d\Delta \lambda_1 - \frac{\partial \mathbf{K}}{\partial \boldsymbol{\kappa}} \frac{\partial j_2}{\partial \mathbf{K}} d\Delta \lambda_2 \end{aligned} \quad (5.39)$$

which gives

$$\begin{aligned} f_1(\boldsymbol{\sigma}_{i+1}^C, \mathbf{K}_i^C) &= f_1(\boldsymbol{\sigma}_i^C, \mathbf{K}_{i+1}^C) - \mathbf{a}_1^T \mathbf{T}\mathbf{r}(\boldsymbol{\sigma}_i^C, \Delta \lambda_{1,i}, \Delta \lambda_{2,i}) - \mathbf{a}_1^T \mathbf{D}^c \mathbf{b}_1 d\Delta \lambda_2 - \mathbf{a}_1^T \mathbf{D}^c \mathbf{b}_2 d\Delta \lambda_2 - \\ &\quad \left( \frac{\partial f_1}{\partial \mathbf{K}} \right)^T \left( \frac{\partial \mathbf{K}}{\partial \boldsymbol{\kappa}} \frac{\partial \boldsymbol{\kappa}}{\partial \Delta \lambda_1} d\Delta \lambda_1 + \frac{\partial \mathbf{K}}{\partial \boldsymbol{\kappa}} \frac{\partial \boldsymbol{\kappa}}{\partial \Delta \lambda_2} d\Delta \lambda_2 \right) \end{aligned} \quad (5.40)$$

and similarly for  $f_2$

$$\begin{aligned} f_2(\boldsymbol{\sigma}_{i+1}^C, \mathbf{K}_i^C) &= f_2(\boldsymbol{\sigma}_i^C, \mathbf{K}_{i+1}^C) - \mathbf{a}_2^T \mathbf{T}\mathbf{r}(\boldsymbol{\sigma}_i^C, \Delta \lambda_{1,i}, \Delta \lambda_{2,i}) - \mathbf{a}_2^T \mathbf{D}^c \mathbf{b}_1 d\Delta \lambda_2 - \mathbf{a}_2^T \mathbf{D}^c \mathbf{b}_2 d\Delta \lambda_2 - \\ &\quad \left( \frac{\partial f_2}{\partial \mathbf{K}} \right)^T \left( \frac{\partial \mathbf{K}}{\partial \boldsymbol{\kappa}} \frac{\partial \boldsymbol{\kappa}}{\partial \Delta \lambda_1} d\Delta \lambda_1 + \frac{\partial \mathbf{K}}{\partial \boldsymbol{\kappa}} \frac{\partial \boldsymbol{\kappa}}{\partial \Delta \lambda_2} d\Delta \lambda_2 \right) \end{aligned} \quad (5.41)$$

Equating (5.40) and (5.41) with 0, leads to two equations with two unknowns, namely  $d\Delta \lambda_1$  and  $d\Delta \lambda_2$  which can be found. Once  $d\Delta \lambda_1$  and  $d\Delta \lambda_2$  are obtained,  $d\boldsymbol{\sigma}$  can be found using (5.36), which leads to a new  $\boldsymbol{\sigma}_{i+1}^C$ . Further  $\Delta \lambda_1$  and  $\Delta \lambda_2$  are updated by

$$\Delta \lambda_{1,i+1} = \Delta \lambda_{1,i} + d\Delta \lambda \quad (5.42)$$

$$\Delta \lambda_{2,i+1} = \Delta \lambda_{2,i} + d\Delta \lambda \quad (5.43)$$

And new values of  $d\Delta \lambda_1$  and  $d\Delta \lambda_2$  can again be found. The above-mentioned steps are repeated until satisfactory precision is reached.

### 5.4.1 Consistent constitutive matrix

The consistent constitutive matrix of a point belonging to two active yield functions is found in much the same was as it was found for the point belonging to one yield function, namely by taking the derivative of (5.8) and utilizing (5.24)

$$\frac{d\Delta\sigma}{d\Delta\epsilon} = \frac{dD\Delta\epsilon}{d\Delta\epsilon} - \frac{\partial\Delta\lambda_1 D\mathbf{b}_1}{\partial\Delta\lambda_1} \cdot \frac{d\Delta\lambda_1}{d\Delta\epsilon} - \frac{\partial\Delta\lambda_1 D\mathbf{b}_1}{\partial\Delta\sigma} \cdot \frac{d\Delta\sigma}{d\Delta\epsilon} - \frac{\partial\Delta\lambda_2 D\mathbf{b}_2}{\partial\Delta\lambda_2} \cdot \frac{d\Delta\lambda_2}{d\Delta\epsilon} - \frac{\partial\Delta\lambda_2 D\mathbf{b}_2}{\partial\Delta\sigma} \cdot \frac{d\Delta\sigma}{d\Delta\epsilon} \quad (5.44)$$

which can be rewritten to

$$d\Delta\sigma = \mathbf{T}\mathbf{D}(d\Delta\epsilon - d\Delta\lambda_1 \mathbf{b}_1 - d\Delta\lambda_2 \mathbf{b}_2) \quad (5.45)$$

Using the consistency condition of both yield criteria together with equation (5.36) and (5.39), results in

$$\begin{aligned} \mathbf{a}_1^T d\Delta\sigma + \left( \frac{\partial f_1}{\partial \mathbf{K}} \right)^T d\mathbf{K} &= \mathbf{a}_1^T \mathbf{T}\mathbf{D}(d\Delta\epsilon - d\Delta\lambda_1 \mathbf{b}_1 - d\Delta\lambda_2 \mathbf{b}_2) - \\ &\quad \left( \frac{\partial f_1}{\partial \mathbf{K}} \right)^T \left( \frac{\partial \mathbf{K}}{\partial \boldsymbol{\kappa}} \frac{\partial j_1}{\partial \mathbf{K}} d\Delta\lambda_1 + \frac{\partial \mathbf{K}}{\partial \boldsymbol{\kappa}} \frac{\partial j_2}{\partial \mathbf{K}} d\Delta\lambda_2 \right) = 0 \end{aligned} \quad (5.46)$$

$$\begin{aligned} \mathbf{a}_2^T d\Delta\sigma + \left( \frac{\partial f_2}{\partial \mathbf{K}} \right)^T d\mathbf{K} &= \mathbf{a}_2^T \mathbf{T}\mathbf{D}(d\Delta\epsilon - d\Delta\lambda_1 \mathbf{b}_1 - d\Delta\lambda_2 \mathbf{b}_2) - \\ &\quad \left( \frac{\partial f_2}{\partial \mathbf{K}} \right)^T \left( \frac{\partial \mathbf{K}}{\partial \boldsymbol{\kappa}} \frac{\partial j_1}{\partial \mathbf{K}} d\Delta\lambda_1 + \frac{\partial \mathbf{K}}{\partial \boldsymbol{\kappa}} \frac{\partial j_2}{\partial \mathbf{K}} d\Delta\lambda_2 \right) = 0 \end{aligned} \quad (5.47)$$

This can also be written as

$$\begin{bmatrix} \mathbf{a}_1^T \mathbf{D}^c \Delta\epsilon \\ \mathbf{a}_2^T \mathbf{D}^c \Delta\epsilon \end{bmatrix} - \mathbf{A} \begin{bmatrix} d\lambda_1 \\ d\lambda_2 \end{bmatrix} = \begin{bmatrix} 0 \\ 0 \end{bmatrix} \quad (5.48)$$

where

$$\mathbf{A} = \begin{bmatrix} A_{11} & A_{12} \\ A_{21} & A_{22} \end{bmatrix} \quad (5.49)$$

$$A_{ik} = \mathbf{a}_i^T \mathbf{D}^c \mathbf{b}_k + \left( \frac{\partial f_i}{\partial \mathbf{K}} \right)^T \frac{\partial \mathbf{K}}{\partial \boldsymbol{\kappa}} \frac{\partial j_k}{\partial \mathbf{K}} \quad (5.50)$$

Thus,  $d\lambda_1$  and  $d\lambda_2$  can be found to be

$$\begin{bmatrix} d\lambda_1 \\ d\lambda_2 \end{bmatrix} = \mathbf{B} \begin{bmatrix} \mathbf{a}_1^T \mathbf{D}^c d\Delta\epsilon \\ \mathbf{a}_2^T \mathbf{D}^c d\Delta\epsilon \end{bmatrix} \quad (5.51)$$

where

$$\mathbf{B} = \mathbf{A}^{-1} = \begin{bmatrix} B_{11} & B_{12} \\ B_{21} & B_{22} \end{bmatrix} \quad (5.52)$$

Substituting back into (5.45) gives

$$\begin{aligned} d\Delta\sigma &= \mathbf{D}^c (d\Delta\epsilon - B_{11} \mathbf{a}_1^T \mathbf{D}^c d\Delta\epsilon \mathbf{b}_1 - B_{12} \mathbf{a}_2^T \mathbf{D}^c d\Delta\epsilon \mathbf{b}_1 \\ &\quad - B_{21} \mathbf{a}_1^T \mathbf{D}^c d\Delta\epsilon \mathbf{b}_2 - B_{22} \mathbf{a}_2^T \mathbf{D}^c d\Delta\epsilon \mathbf{b}_2) \end{aligned} \quad (5.53)$$

Using (5.53),  $\mathbf{D}^{epc}$  can be derived to

$$\mathbf{D}^{epc} = \mathbf{D}^c - B_{11} \mathbf{b}_1 \mathbf{a}_1^T \mathbf{D}^c - B_{12} \mathbf{b}_1 \mathbf{a}_2^T \mathbf{D}^c - B_{21} \mathbf{b}_2 \mathbf{a}_1^T \mathbf{D}^c - B_{22} \mathbf{b}_2 \mathbf{a}_2^T \mathbf{D}^c \quad (5.54)$$

which can also be written as

$$\mathbf{D}^{epc} = \mathbf{D}^c - \sum_{i=1}^2 \sum_{j=1}^2 B_{ij} \mathbf{b}_i \mathbf{a}_j^T \mathbf{D}^c \quad (5.55)$$

If needed, the infinitesimal constitutive matrix is found by replacing  $\mathbf{D}^c$  in (5.55) with  $\mathbf{D}$ .

## 5.5 Return to Three Active Yield Functions

An updated stress state might also be returned to the intersection of three yield surfaces,  $f_1$ ,  $f_2$  and  $f_3$ , with the plastic potentials  $g_1$ ,  $g_2$  and  $g_3$  and the hardening potentials  $j_1$ ,  $j_2$  and  $j_3$ . This scenario is very similar to the scenario with two active yield surfaces, which was discussed in the previous section, and will only be touched upon briefly. The plastic corrector is given by

$$\Delta\boldsymbol{\sigma}^P = \Delta\lambda_1 \mathbf{D} \mathbf{b}_1|_C + \Delta\lambda_2 \mathbf{D} \mathbf{b}_2|_C + \Delta\lambda_3 \mathbf{D} \mathbf{b}_3|_C \quad (5.56)$$

and the evolution law is assumed to be given by

$$\boldsymbol{\kappa}^C = \boldsymbol{\kappa}^A - \Delta\lambda_1 \left. \frac{\partial j_1}{\partial \mathbf{K}} \right|_C - \Delta\lambda_2 \left. \frac{\partial j_2}{\partial \mathbf{K}} \right|_C - \Delta\lambda_3 \left. \frac{\partial j_3}{\partial \mathbf{K}} \right|_C \quad (5.57)$$

The return algorithm is almost identical to the one mentioned in the previous section, except that an extra unknown,  $\Delta\lambda_3$  needs to be found, which is possible because of the extra equation introduced by the consistency condition of the third yield criterion. The derivation of this procedure is omitted, however the modification matrix,  $\mathbf{T}$ , is given by

$$\mathbf{T} = \left( \mathbf{I} + \Delta\lambda_1 \mathbf{D} \frac{\partial \mathbf{b}_1}{\partial \boldsymbol{\sigma}} + \Delta\lambda_2 \mathbf{D} \frac{\partial \mathbf{b}_2}{\partial \boldsymbol{\sigma}} + \Delta\lambda_3 \mathbf{D} \frac{\partial \mathbf{b}_3}{\partial \boldsymbol{\sigma}} \right)^{-1} \quad (5.58)$$

Similarly, the consistent constitutive matrix can be found to be given by

$$\mathbf{D}^{epc} = \mathbf{D}^c - \sum_{i=1}^3 \sum_{j=1}^3 B_{ij} \mathbf{b}_i \mathbf{a}_j^T \mathbf{D}^c \quad (5.59)$$

where  $\mathbf{B}$  is the  $3 \times 3$  equivalent matrix to the one in the previous section.

## 5.6 Determination of Correct Return Type

In the general six-dimensional stress space, there is no easy way of determining, which of the above mentioned return algorithms, that should be applied to a certain predictor stress. Because of this, a commonly used strategy is to start out with returning to a single yield surface. The updated stress state is then evaluated based upon some specific requirements. In case these requirements are not met, the predictor stress is returned using a return to two yield surfaces and so on. In general stress space, it is theoretically possible, that an updated stress state has to be returned using as much as six active yield surfaces. However, in the three dimensional principal stress space, geometric arguments can be applied, to establish which method is to be applied.

## Return Mapping in Principal Stress Space

If the material in question is isotropic, the stress states within the material can be expressed in principal stresses through a coordinate transformation, see Figure 6.1. Thus the updated stress state can be

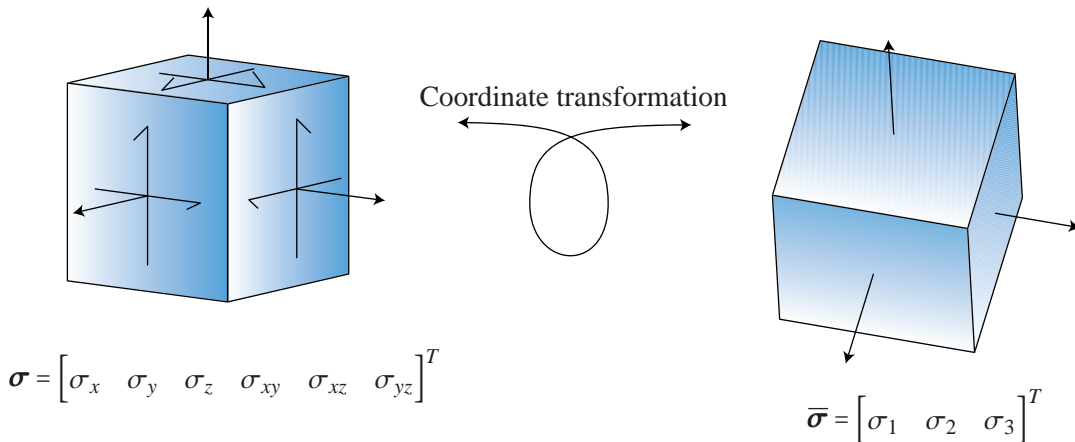


Figure 6.1: Coordinate transformation of general stress space into principal stress space

found in principal stress space, and only the three principal stresses need to be found. And since only three values are involved, the problem can be visualized in 3D space, where advantages can be made of geometrical arguments, which can be used to simplify the expressions used in chapter 5. The drawback is, that coordinate transformation calculations have to be performed. The predictor stress,  $\boldsymbol{\sigma}^B$ , is transformed into principal stresses using ordinary coordinate transformation. Afterwards, the updated principal stress state,  $\bar{\boldsymbol{\sigma}}^C$ , and the consistent constitutive matrix aligned with the principal axes,  $\hat{\mathbf{D}}^{epc}$ , is found and then transformed back into the original coordinate system of the model, cf. Table 6.1.

The derivations of chapter 5 should of course still hold in principal stress space for an isotropic material. However,  $\boldsymbol{\sigma}$  is reduced from the six components of (1.2) to only three components, namely

$$\bar{\boldsymbol{\sigma}} = \begin{bmatrix} \sigma_1 & \sigma_2 & \sigma_3 \end{bmatrix}^T \quad (6.1)$$

where the overbar,  $\bar{\cdot}$ , is used to indicate, that we are dealing with principal stresses.

○ $\sigma^B \rightarrow \bar{\sigma}^B$	Transform predicted stress state into principal stresses
○ $\bar{\sigma}^C(\bar{\sigma}^B)$	Find the updated principal stress state
○ $\hat{D}^{epc}(\bar{\sigma}^C)$	Find consistent constitutive matrix aligned with principal axes
○ $\bar{\sigma}^C \rightarrow \sigma^C$	Transform updated principal stress state to general stresses aligned with model axes
○ $\hat{D}^{epc} \rightarrow D^{epc}$	Transform consistent constitutive matrix into general stresses aligned with model axes

Table 6.1: Schematic of return mapping in principal stress space.

## 6.1 Modificaton Matrix

The modification matrix used in finding the consistent constitutive matrix,  $\mathbf{T}$ , is still created as a full  $6 \times 6$  matrix, however, it is aligned with the principal stress axes, meaning that  $\sigma_x$  is in the same direction as  $\sigma_1$ ,  $\sigma_y$  is in the same direction as  $\sigma_2$  and  $\sigma_z$  is in the direction of  $\sigma_3$ . This is denoted by a hat,  $\hat{\cdot}$ .  $\hat{\mathbf{T}}$  is divided into two parts

$$\hat{\mathbf{T}} = \begin{bmatrix} \bar{\mathbf{T}} & \mathbf{0} \\ \mathbf{0} & \tilde{\mathbf{T}} \end{bmatrix} \quad (6.2)$$

where  $\bar{\mathbf{T}}$  relates to the principal stresses and  $\tilde{\mathbf{T}}$  relates to the shear stresses. For a return to a yield surface using (5.22) results in

$$\bar{\mathbf{T}} = \left( \bar{\mathbf{I}} + \Delta\lambda \bar{\mathbf{D}} \frac{\partial \bar{\mathbf{b}}}{\partial \bar{\sigma}} \right)^{-1} \quad (6.3)$$

and for a return to two yield surfaces using (5.37) results in

$$\bar{\mathbf{T}} = \left( \bar{\mathbf{I}} + \Delta\lambda_1 \bar{\mathbf{D}} \frac{\partial \bar{\mathbf{b}}_1}{\partial \bar{\sigma}} + \Delta\lambda_2 \bar{\mathbf{D}} \frac{\partial \bar{\mathbf{b}}_2}{\partial \bar{\sigma}} \right)^{-1} \quad (6.4)$$

and so on. Further,  $\tilde{\mathbf{T}}$  is given by [Clausen et al., 2006]

$$\tilde{\mathbf{T}} = \begin{bmatrix} \frac{\sigma_1^C - \sigma_2^C}{\sigma_1^B - \sigma_2^B} & & \\ & \frac{\sigma_1^C - \sigma_3^C}{\sigma_1^B - \sigma_3^B} & \\ & & \frac{\sigma_2^C - \sigma_3^C}{\sigma_2^B - \sigma_3^B} \end{bmatrix} \quad (6.5)$$

Once  $\hat{\mathbf{T}}$  is found, the consistent constitutive matrix aligned with the principal axes,  $\hat{\mathbf{D}}^{epc}$ , is calculated analogous to equation (5.23), (5.55), or (5.59), except that  $\mathbf{a}$ ,  $\mathbf{b}$  and  $\mathbf{D}^c$  is replaced by

$$\hat{\mathbf{a}} = \begin{bmatrix} \bar{\mathbf{a}}^T & 0 & 0 & 0 \end{bmatrix}^T \quad (6.6)$$

$$\hat{\mathbf{b}} = \begin{bmatrix} \bar{\mathbf{b}}^T & 0 & 0 & 0 \end{bmatrix}^T \quad (6.7)$$

$$\hat{\mathbf{D}}^c = \hat{\mathbf{T}} \mathbf{D}^c \quad (6.8)$$

## 6.2 Boundary Planes

As mentioned earlier, the principal stress space is a three dimensional space in which the yield criterion can be visualized. Further, from (5.13), it is known, that if a predicted stress state should be returned to a surface, the direction,  $\bar{s}$ , see Figure 6.2, of the plastic corrector,  $\Delta\sigma^p$ , is given by

$$\bar{s} = \overline{D\bar{b}} \quad (6.9)$$

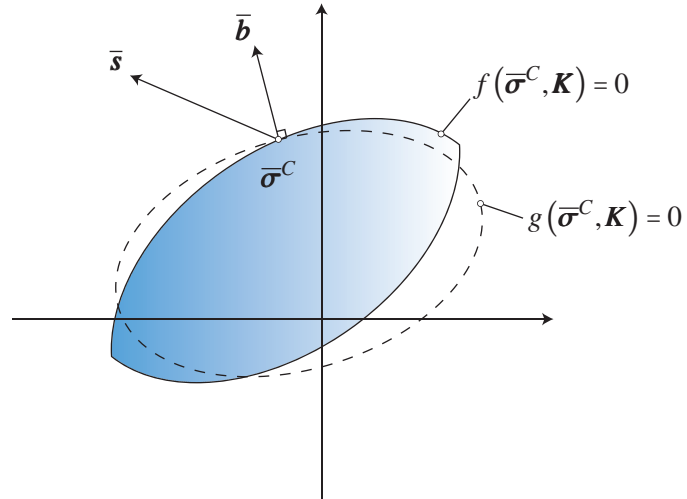


Figure 6.2: Direction of the plastic corrector of a return with one active yield function

By evaluating this expression along the boundaries of the yield surface, the predictor stress states, which can be returned to the yield surface is outlined. The principle is shown for a Mohr-Coulomb criterion on Figure 6.3. The stress space within these boundaries is known as a return region, belonging to the specific yield surface.

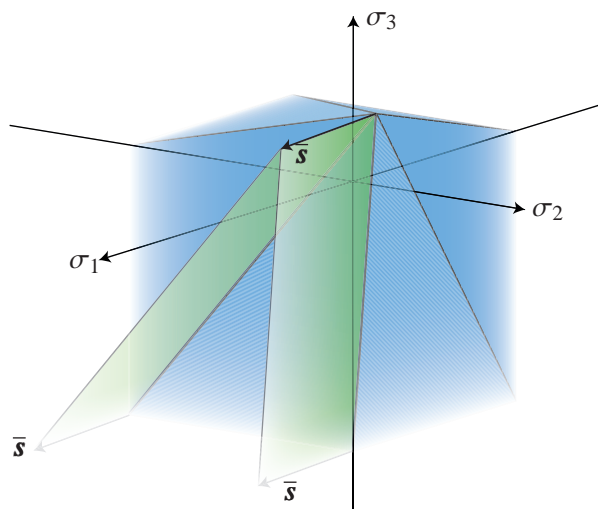


Figure 6.3: Outlining of a return region by the use of boundary planes.

Similarly, the direction of the plastic corrector for a predictor stress which is to be returned to two active yield surfaces, see Figure 6.4, is given by

$$\bar{s} = \eta \bar{s}_1 + \rho \bar{s}_2 \quad (6.10)$$

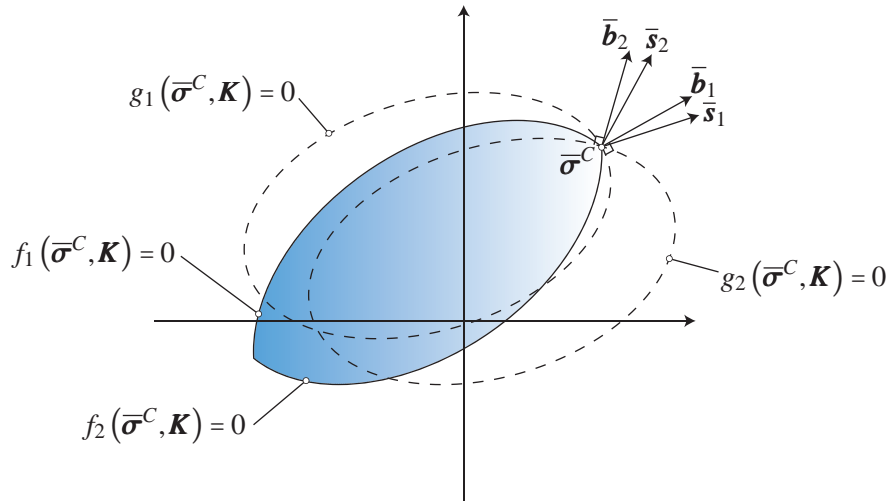


Figure 6.4: *Direction of the plastic corrector of a return with two active yield functions is a linear combination of the two plastic corrector directions involved*

where  $\eta$  and  $\rho$  are some arbitrary positive scalars. Similar arguments apply for a predictor stress with three active yield surfaces and so on. With this knowledge, it is possible to determine which part of the yield criterion, a specific predictor stress state should be returned to. Further, if the plastic potential is linear, the different return regions are made up of planes, since  $\bar{s}$  is independent of the position in yield space. With this knowledge, it is possible to determine the correct return algorithm, without the trial-and-error approach of the general stress space updating scheme.

# Implementation of Strain Hardening Mohr-Coulomb Model

In this chapter, the theory of the previous chapters will be applied to a Mohr-Coulomb model using linear elasticity, non-associated plasticity and isotropic strain hardening, along with the evolution laws of equation (4.25) and (4.31).

## 7.1 Basic Premises

As mentioned in chapter 3, the Mohr-Coulomb yield criterion can take the form of

$$f(\boldsymbol{\sigma}, \sigma_c, k) = k\sigma_1 - \sigma_3 - \sigma_c = 0 \quad (7.1)$$

which will be used in the current implementation due to its simplicity compared to (3.5). The yield criterion is a function of both the friction angle,  $\varphi$ , and the cohesion  $c$ . In this implementation, it is assumed, that the friction angle remains constant. Thus, the hardening parameters vector,  $\mathbf{K}$ , simplifies to a scalar, namely the cohesion,  $c$ . Further the state parameters vector,  $\boldsymbol{\kappa}$ , of the material, is chosen to be the scalar accumulated plastic strain,  $\bar{\varepsilon}^P$ . Thus

$$\mathbf{K}(\boldsymbol{\kappa}) = c(\bar{\varepsilon}^P) \quad (7.2)$$

The plastic potential,  $g$ , is chosen as

$$g = (\boldsymbol{\sigma}, c, \psi) = \sigma_1 - \sigma_3 + (\sigma_1 + \sigma_3) \sin(\psi) - 2c \cos(\psi) \quad (7.3)$$

where  $\psi$  represents the angle of dilation. The evolution of the accumulated plastic strain is given by the hardening potential function,  $j$ , cf. equation (4.25), and is chosen as

$$j = (\boldsymbol{\sigma}, c, \varphi) = \sigma_1 - \sigma_3 + (\sigma_1 + \sigma_3) \sin(\varphi) - 2c \cos(\varphi) \quad (7.4)$$

## 7.2 Derivatives

The derivative of  $f$  with respect to  $\bar{\sigma}$  is given by

$$\bar{\mathbf{a}} = \frac{\partial f}{\partial \bar{\sigma}} = \begin{bmatrix} k \\ 0 \\ -1 \end{bmatrix} \quad (7.5)$$

The derivative of  $f$  with respect to the hardening variable,  $c$ , is given by

$$\frac{\partial f}{\partial \mathbf{K}} = \frac{\partial f}{\partial c} = \frac{\partial f}{\partial \sigma_c} \frac{d\sigma_c}{dc} = -2\sqrt{k} \quad (7.6)$$

The derivative of  $g$  with respect to  $\bar{\sigma}$  is given by

$$\bar{\mathbf{b}} = \frac{\partial g}{\partial \bar{\sigma}} = \begin{bmatrix} 1 + \sin(\psi) \\ 0 \\ -1 + \sin(\psi) \end{bmatrix} \quad (7.7)$$

The derivative of  $j$  with respect to the hardening variables is given by

$$\frac{\partial j}{\partial \mathbf{K}} = \frac{\partial j}{\partial c} = -2\cos(\varphi) \quad (7.8)$$

Finally, the derivative of the hardening parameters,  $\mathbf{K}$ , with respect to the state parameters,  $\kappa$ , is given by

$$\frac{\partial \mathbf{K}}{\partial \kappa} = \frac{\partial c}{\partial \bar{\varepsilon}^P} = H \quad (7.9)$$

where  $H$  is the gradient of the chosen  $\bar{\varepsilon}^P - c$ -curve at the current point of accumulated plastic strain. This curve could be modeled as a function, however, in the current implementation, it is defined by a number of predefined  $(\bar{\varepsilon}^P, c)$  points, which makes it possible to choose an arbitrary curve, without changing the computer code. The specific value of  $c$  and  $H$  is interpolated between these points, see Figure 7.1. Using this approach, the model is able to handle all of the hardening models shown in Figure 1.1 as well as the elastic brittle behavior shown in Figure 1.2.

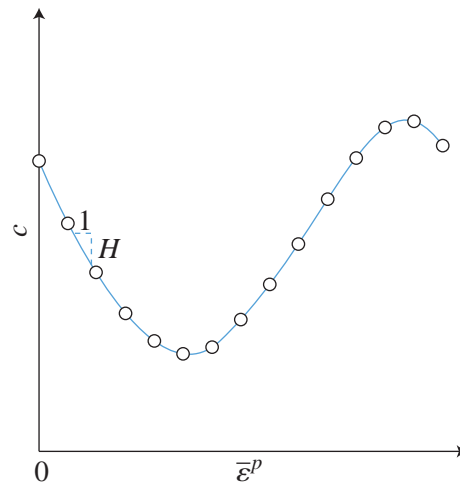


Figure 7.1: Example of arbitrary  $\bar{\varepsilon}^P - c$ -curve defined by a set of  $(\bar{\varepsilon}^P, c)$  points.

### 7.3 Yield Criterion Regions

As shown in Figure 3.2, the Mohr-Coulomb yield criterion consists of six yield surfaces in principal stress space. However, if by definition,  $\sigma_1$  is the major principal stress, and  $\sigma_3$  is the minor principal

stress when transforming the general stress state into principal stress space, it is only necessary to operate with the yield surface, that satisfies this condition, named  $f_1$ , and the two neighboring yield surfaces,  $f_2$  and  $f_6$ . See Figure 7.2.

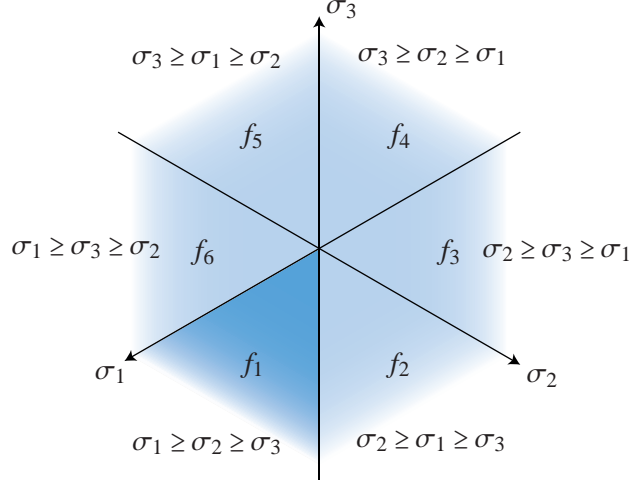


Figure 7.2: The Mohr-Coulomb criterion seen from the hydrostatic axis. The primary yield surface,  $f_1$ , is shown in blue, while the remaining yield surfaces are faded out.

$f_1, f_2$  and  $f_6$  is given by

$$f_1(\boldsymbol{\sigma}, \sigma_c, k) = k\sigma_1 - \sigma_3 - \sigma_c = 0 \quad (7.10)$$

$$f_2(\boldsymbol{\sigma}, \sigma_c, k) = k\sigma_2 - \sigma_3 - \sigma_c = 0 \quad (7.11)$$

$$f_6(\boldsymbol{\sigma}, \sigma_c, k) = k\sigma_1 - \sigma_2 - \sigma_c = 0 \quad (7.12)$$

Ie.  $\sigma_1$  is switched with  $\sigma_2$  for yield surface  $f_2$ , and  $\sigma_3$  is switched with  $\sigma_2$  for yield surface  $f_6$ . This leads to the following derivatives

$$\bar{\mathbf{a}}_1 = \begin{bmatrix} k \\ 0 \\ -1 \end{bmatrix} \quad \bar{\mathbf{a}}_2 = \begin{bmatrix} 0 \\ k \\ -1 \end{bmatrix} \quad \bar{\mathbf{a}}_6 = \begin{bmatrix} k \\ -1 \\ 0 \end{bmatrix} \quad (7.13)$$

The index swapping is also valid for the plastic and hardening potentials belonging to these yield surfaces. Thus, the plastic strain direction is given by

$$\bar{\mathbf{b}}_1 = \begin{bmatrix} 1 + \sin(\psi) \\ 0 \\ -1 + \sin(\psi) \end{bmatrix} \quad \bar{\mathbf{b}}_2 = \begin{bmatrix} 0 \\ 1 + \sin(\psi) \\ -1 + \sin(\psi) \end{bmatrix} \quad \bar{\mathbf{b}}_6 = \begin{bmatrix} 1 + \sin(\psi) \\ -1 + \sin(\psi) \\ 0 \end{bmatrix} \quad (7.14)$$

The intersection between yield surface  $f_1$  and  $f_2$  is a line in principal stress space denoted  $l_1$ , see Figure 7.3. Along this line  $\sigma_1 = \sigma_2$  and is thus given by

$$\bar{\boldsymbol{\sigma}}_{l_1} = \begin{bmatrix} \sigma_1 \\ \sigma_1 \\ k\sigma_1 - \sigma_c \end{bmatrix} \quad (7.15)$$

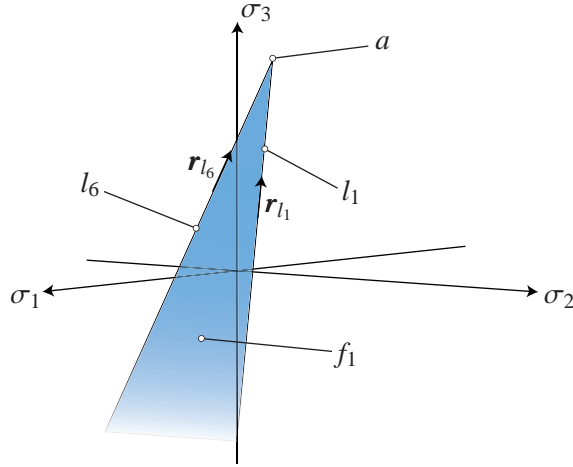


Figure 7.3: Naming convention for the Mohr-Coulomb criterion.

Similarly, the intersection between  $f_1$  and  $f_6$  is denoted  $l_6$  where  $\sigma_2 = \sigma_3$ , and is given by

$$\bar{\boldsymbol{\sigma}}_{l_6} = \begin{bmatrix} \sigma_1 \\ k\sigma_1 - \sigma_c \\ k\sigma_1 - \sigma_c \end{bmatrix} \quad (7.16)$$

The intersection of  $f_1$ ,  $f_2$  and  $f_6$  is a point in principal stress space, and is denoted  $a$ , given by

$$\bar{\boldsymbol{\sigma}}_a = \frac{\sigma_c}{k-1} \begin{bmatrix} 1 \\ 1 \\ 1 \end{bmatrix} \quad (7.17)$$

Any predicted stress state falling outside the yield criterion is to be returned to either the primary yield surface,  $f_1$ , the yield lines,  $l_1$  or  $l_6$ , or the apex,  $a$ .

## 7.4 Return Regions and Boundaries

The region of principal stress space, that returns to  $f_1$  is denominated  $R_{f_1}$ . Stress points which are to be returned to  $l_1$  is denominated  $R_{l_1}$  and similarly for  $R_{l_6}$  and  $R_a$ . Due to the linearity of the Mohr Coulomb criterion, the different return regions are bounded by planes. Based on the predictor stress state's location relative to these planes, the correct return region can be established and hence the correct return algorithm can be applied. A plane can be defined by it's normal vector,  $\mathbf{n}$ , and a point belonging to the plane,  $\mathbf{x}_0$ , as

$$\mathbf{n}^T (\mathbf{x} - \mathbf{x}_0) = 0 \quad (7.18)$$

Any vector,  $\mathbf{x}$ , for which the above is satisfied is situated on the plane. A point lying below the plane gives a negative number, and a point lying above the plane results in a positive number. Thus, it is necessary to identify the normals of each plane, which can be calculated based on the directions, in which the planes span.

The plastic corrector direction belonging to a surface return to yield surface  $f_1$  is given by

$$\bar{s}_1 = \bar{D}\bar{b}_1 = -\frac{E}{(1+\nu)(2\nu-1)} \begin{bmatrix} 1 + \sin(\varphi) - 2\nu \\ 2\nu\sin(\varphi) \\ 2\nu - 1 + \sin(\varphi) \end{bmatrix} \quad (7.19)$$

and the intersection between the  $f_1$ -yield surface and the  $f_2$ -yield surface is fully determined by  $\bar{\sigma}_{l_1}$ , (7.15), which by differentiation gives the direction of the intersection line,  $\mathbf{r}_{l_1}$ , see Figure 7.3,

$$\mathbf{r}_{l_1} = \frac{\partial \bar{\sigma}_{l_1}}{\partial \sigma_1} = \begin{bmatrix} 1 \\ 1 \\ k \end{bmatrix} \quad (7.20)$$

By taking the cross product between  $\mathbf{r}_{l_1}$  and  $\bar{s}_1$ , the normal of the plane separating the return region belonging to yield surface  $f_1$ , and those belonging to line  $l_1$  can be established as

$$\mathbf{n}_{R_{f_1} \rightarrow R_{l_1}} = \bar{s}_1 \times \mathbf{r}_{l_1} \quad (7.21)$$

where the arrow designates, that the normal of the plane is pointing from the region belonging to  $f_1$ , to the region belonging to  $l_1$ . Similarly, the direction of  $l_6$  is given by

$$\mathbf{r}_{l_6} = \frac{\partial \bar{\sigma}_{l_6}}{\partial \sigma_1} = \begin{bmatrix} 1 \\ k \\ k \end{bmatrix} \quad (7.22)$$

and thus the normal of the plane which creates the boundary between the region of predictor stresses belonging to  $f_1$  and those belonging to  $l_6$  can be found to give

$$\mathbf{n}_{R_{l_6} \rightarrow R_{f_1}} = \bar{s}_1 \times \mathbf{r}_{l_6} \quad (7.23)$$

The boundary plane separating  $R_{l_1}$  from  $R_a$  is spanned by the direction of  $\bar{s}_1$  and  $\bar{s}_2$ , which is the plastic corrector direction belonging to  $f_2$ . Thus

$$\mathbf{n}_{R_{l_1} \rightarrow R_a} = \bar{s}_1 \times \bar{s}_2 \quad (7.24)$$

and similarly for the boundary plane which separates  $R_{l_6}$  from  $R_a$

$$\mathbf{n}_{R_{l_6} \rightarrow R_a} = \bar{s}_6 \times \bar{s}_1 \quad (7.25)$$

In order to completely define the boundary planes, a point on each plane is also needed. Since all the planes go through the apex of the criterion, this point is simply chosen to represent all four boundary planes. Based upon this, four boundary planes, see Figure 7.4, can be defined by

$$p_{R_{f_1} \rightarrow R_{l_1}}(\boldsymbol{\sigma}^B) = \mathbf{n}_{R_{f_1} \rightarrow R_{l_1}}^T (\bar{\sigma}^B - \bar{\sigma}_a) = 0 \quad (7.26)$$

$$p_{R_{l_6} \rightarrow R_{f_1}}(\boldsymbol{\sigma}^B) = \mathbf{n}_{R_{l_6} \rightarrow R_{f_1}}^T (\bar{\sigma}^B - \bar{\sigma}_a) = 0 \quad (7.27)$$

$$p_{R_{l_1} \rightarrow R_a}(\boldsymbol{\sigma}^B) = \mathbf{n}_{R_{l_1} \rightarrow R_a}^T (\bar{\sigma}^B - \bar{\sigma}_a) = 0 \quad (7.28)$$

$$p_{R_{l_6} \rightarrow R_a}(\boldsymbol{\sigma}^B) = \mathbf{n}_{R_{l_6} \rightarrow R_a}^T (\bar{\sigma}^B - \bar{\sigma}_a) = 0 \quad (7.29)$$

Using these boundary planes, a rule set can be set up, which determines the correct return algorithm based upon the evaluation of these planes, which has been done in Table 7.1.

Rule #	Conditions	Return to
1	$p_{R_{f_1} \rightarrow R_{l_1}}(\sigma^B) \leq 0 \wedge p_{R_{l_6} \rightarrow R_{f_1}}(\sigma^B) \geq 0$	$f_1$
2	$p_{R_{f_1} \rightarrow R_{l_1}}(\sigma^B) \geq 0 \wedge p_{R_{l_1} \rightarrow R_a}(\sigma^B) \leq 0$	$l_1$
3	$p_{R_{l_6} \rightarrow R_{f_1}}(\sigma^B) \leq 0 \wedge p_{R_{l_6} \rightarrow R_a}(\sigma^B) \leq 0$	$l_6$
4	$p_{R_{l_1} \rightarrow R_a}(\sigma^B) \geq 0 \wedge p_{R_{l_6} \rightarrow R_a}(\sigma^B) \geq 0$	$a$

Table 7.1: Rule set for return algorithms. See Figure 7.4 for further details of boundary plane location and naming.

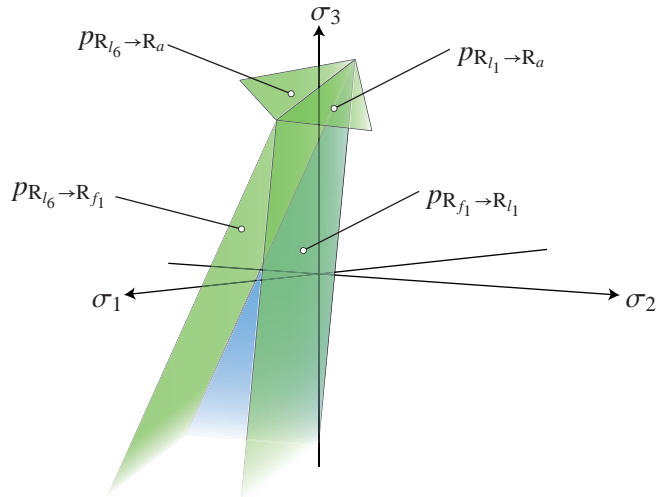


Figure 7.4: Boundary planes of the Mohr-Coulomb criterion. The visible side of each boundary plane in the figure is defined as the positive direction of the normal.

## 7.5 Return Algorithms

The return algorithms used for the Mohr-Coulomb criterion are particularly simple. Because of the linearity of the plastic potential, which has been utilized, the plastic strain direction is independent of the stresses. This means, that the plastic strain direction is the same, whether it is evaluated at the predictor stress point,  $\bar{\sigma}^B$ , or at the updated stress point,  $\bar{\sigma}^C$ . Thus, equation (5.13) can be simplified to

$$\Delta\sigma^P \approx \Delta\lambda D b|_B \quad (7.30)$$

This means, that the only unknown in calculating the plastic corrector,  $\Delta\sigma^P$ , is the plastic multiplier  $\Delta\lambda$ .

### 7.5.1 Return to yield surface $f_1$

If the predictor point qualifies for a return to  $f_1$ , only one yield surface is active, and hence only one plastic multiplier needs to be found. The updated stress state,  $\bar{\sigma}^C$ , is given as

$$\bar{\sigma}^C = \bar{\sigma}^B - \Delta\sigma^P = \bar{\sigma}^B - \Delta\lambda \bar{D} \bar{b}_1 \quad (7.31)$$

which have to satisfy the condition

$$f_1(\bar{\sigma}^C, \sigma_c^C, k) = k\sigma_1^C - \sigma_3^C - \sigma_c^C = 0 \quad (7.32)$$

With the use of equation (7.31),  $\sigma_1^C$  and  $\sigma_3^C$  can be expressed as

$$\sigma_1^C = \sigma_1^B - \Delta\lambda s_{1,1} \quad (7.33)$$

$$\sigma_3^C = \sigma_3^B - \Delta\lambda s_{1,3} \quad (7.34)$$

where  $s_{1,1}$  and  $s_{1,3}$  is the first and third component of  $\bar{s}_1$  respectively. Further, with the use of equation (5.16), the uniaxial compressive strength of the updated stress state,  $\sigma_c^C$ , depends on the accumulated plastic strain at the updated stress state,  $\bar{\varepsilon}^{p,C}$ , which is given as

$$\bar{\varepsilon}^{p,C} = \bar{\varepsilon}^{p,A} - \Delta\lambda \frac{\partial j}{\partial c} = \bar{\varepsilon}^{p,A} + \Delta\lambda 2 \cos(\varphi) \quad (7.35)$$

where equation (7.8) has been used. Thus, the compressive uniaxial strength of the updated stress state,  $\sigma_c^C$ , is given by

$$\sigma_c^C = 2c(\bar{\varepsilon}^{p,C}) \sqrt{k} \quad (7.36)$$

Substituting back into equation (7.32) gives

$$f_1(\Delta\lambda) = k(\sigma_1^B - \Delta\lambda s_{1,1}) - (\sigma_3^B - \Delta\lambda s_{1,3}) - \sigma_c^C = 0 \quad (7.37)$$

which is solved using an ordinary Newton-Raphson iteration procedure with respect to  $\Delta\lambda$ . The gradient of the equation with respect to  $\Delta\lambda$  is

$$\frac{df_1}{d\Delta\lambda} = -ks_{1,1} + s_{1,3} - \frac{d\sigma_c^C}{dc^C} \frac{dc^C}{d\bar{\varepsilon}^{p,C}} \frac{d\bar{\varepsilon}^{p,C}}{d\Delta\lambda} = -ks_{1,1} + s_{1,3} + d\sigma_c \quad (7.38)$$

where

$$d\sigma_c = -\frac{d\sigma_c^C}{dc^C} \frac{dc^C}{d\bar{\varepsilon}^{p,C}} \frac{d\bar{\varepsilon}^{p,C}}{d\Delta\lambda} = 4H \cos(\varphi) \sqrt{k} \quad (7.39)$$

using equation (7.9), (7.35) and (7.36). An initial guess of  $\Delta\lambda$  is made and then updated via

$$\Delta\lambda_{i+1} = \Delta\lambda_i - \left( \frac{df_1}{d\Delta\lambda} \Big|_i \right)^{-1} f_1(\Delta\lambda_i) \quad (7.40)$$

until the required precision is reached.

### 7.5.2 Return to yield lines $l_1$ and $l_6$

Returning to one of the yield lines,  $l_1$  and  $l_6$  is a simple expansion of the procedure used for the  $f_1$  return. However, in this case, the plastic corrector is given by

$$\bar{\sigma}^C = \bar{\sigma}^B - \Delta\sigma^P = \bar{\sigma}^B - \Delta\lambda_1 \bar{D}\bar{b}_1 - \Delta\lambda_2 \bar{D}\bar{b}_2 \quad (7.41)$$

where  $\Delta\lambda_1$  and  $\Delta\lambda_2$  are unknown.  $\bar{\sigma}^C$  has to fulfill both yield criteria. For the  $l_1$  return, this results in

$$f_1(\bar{\sigma}^C, \sigma_c^C, k) = k\sigma_1^C - \sigma_3^C - \sigma_c^C = 0 \quad (7.42)$$

$$f_2(\bar{\sigma}^C, \sigma_c^C, k) = k\sigma_2^C - \sigma_3^C - \sigma_c^C = 0 \quad (7.43)$$

where

$$\sigma_1^C = \sigma_1^B - \Delta\lambda_1 s_{1,1} - \Delta\lambda_2 s_{2,1} \quad (7.44)$$

$$\sigma_2^C = \sigma_2^B - \Delta\lambda_1 s_{1,2} - \Delta\lambda_2 s_{2,2} \quad (7.45)$$

$$\sigma_3^C = \sigma_3^B - \Delta\lambda_1 s_{1,3} - \Delta\lambda_2 s_{2,3} \quad (7.46)$$

The accumulated plastic strain of the updated stress state is given by

$$\bar{\varepsilon}^{p,C} = \bar{\varepsilon}^{p,A} - \sum_{i=1}^2 \Delta\lambda_i \frac{\partial j_i}{\partial c} = \bar{\varepsilon}^{p,A} - 2 \cos(\varphi) (\Delta\lambda_1 + \Delta\lambda_2) \quad (7.47)$$

The two yield criteria are embedded in the residual vector  $\mathbf{F}$  as

$$\begin{aligned} \mathbf{F}(\Delta\lambda) &= \begin{bmatrix} f_1(\Delta\lambda_1, \Delta\lambda_2) \\ f_2(\Delta\lambda_1, \Delta\lambda_2) \end{bmatrix} \\ &= \begin{bmatrix} k(\sigma_1^B - \Delta\lambda_1 s_{1,1} - \Delta\lambda_2 s_{2,1}) - (\sigma_3^B - \Delta\lambda_1 s_{1,3} - \Delta\lambda_2 s_{2,3}) - \sigma_c^C \\ k(\sigma_2^B - \Delta\lambda_1 s_{1,2} - \Delta\lambda_2 s_{2,2}) - (\sigma_3^B - \Delta\lambda_1 s_{1,3} - \Delta\lambda_2 s_{2,3}) - \sigma_c^C \end{bmatrix} = \begin{bmatrix} 0 \\ 0 \end{bmatrix} \end{aligned} \quad (7.48)$$

where

$$\Delta\lambda = \begin{bmatrix} \Delta\lambda_1 \\ \Delta\lambda_2 \end{bmatrix} \quad (7.49)$$

The gradient is found to be

$$\frac{\partial \mathbf{F}}{\partial \Delta\lambda^T} = \begin{bmatrix} -ks_{1,1} + s_{1,3} + d\sigma_c & -ks_{2,1} + s_{2,3} + d\sigma_c \\ -ks_{1,2} + s_{1,3} + d\sigma_c & -ks_{2,2} + s_{2,3} + d\sigma_c \end{bmatrix} \quad (7.50)$$

where  $d\sigma_c$  is given by (7.39). The system of equations is solved using a Newton-Raphson iteration, where an initial guess of  $\Delta\lambda$  is made, an afterwards updated as

$$\Delta\lambda_{i+1} = \Delta\lambda_i - \left( \frac{\partial \mathbf{F}}{\partial \Delta\lambda^T} \Big|_i \right)^{-1} \mathbf{F}(\Delta\lambda_i) \quad (7.51)$$

until the required precision is reached. The return algorithm for the  $l_6$  return is analogous to the above, except that the  $f_2$  yield surface is replaced by the  $f_6$  yield surface. This gives

$$\begin{aligned} \mathbf{F}(\Delta\lambda) &= \begin{bmatrix} f_1(\Delta\lambda_1, \Delta\lambda_2) \\ f_6(\Delta\lambda_1, \Delta\lambda_2) \end{bmatrix} \\ &= \begin{bmatrix} k(\sigma_1^B - \Delta\lambda_1 s_{1,1} - \Delta\lambda_2 s_{2,1}) - (\sigma_3^B - \Delta\lambda_1 s_{1,3} - \Delta\lambda_2 s_{2,3}) - \sigma_c^C \\ k(\sigma_1^B - \Delta\lambda_1 s_{1,1} - \Delta\lambda_2 s_{2,1}) - (\sigma_2^B - \Delta\lambda_1 s_{1,2} - \Delta\lambda_2 s_{2,2}) - \sigma_c^C \end{bmatrix} = \begin{bmatrix} 0 \\ 0 \end{bmatrix} \end{aligned} \quad (7.52)$$

with the corresponding gradient

$$\frac{\partial \mathbf{F}}{\partial \Delta\lambda^T} = \begin{bmatrix} -ks_{1,1} + s_{1,3} + d\sigma_c & -ks_{2,1} + s_{2,3} + d\sigma_c \\ -ks_{1,1} + s_{1,2} + d\sigma_c & -ks_{2,1} + s_{2,2} + d\sigma_c \end{bmatrix} \quad (7.53)$$

### 7.5.3 Return to apex point $a$

The return algorithm to the apex of the Mohr-Coulomb criterion is a further expansion of the  $l_1$  and  $l_6$  algorithms, in which case  $f_1$ ,  $f_2$  and  $f_3$  needs to be fulfilled. The approach is similar to the above and

only the main results will be given here. The residual vector is found to be given by

$$\begin{aligned} \mathbf{F}(\Delta\boldsymbol{\lambda}) &= \begin{bmatrix} f_1(\Delta\lambda_1, \Delta\lambda_2, \Delta\lambda_3) \\ f_2(\Delta\lambda_1, \Delta\lambda_2, \Delta\lambda_3) \\ f_6(\Delta\lambda_1, \Delta\lambda_2, \Delta\lambda_3) \end{bmatrix} \\ &= \begin{bmatrix} k(\sigma_1^B - \Delta\lambda_1 s_{1,1} - \Delta\lambda_2 s_{2,1} - \Delta\lambda_3 s_{3,1}) - (\sigma_3^B - \Delta\lambda_1 s_{1,3} - \Delta\lambda_2 s_{2,3} - \Delta\lambda_3 s_{3,3}) - \sigma_c^C \\ k(\sigma_2^B - \Delta\lambda_1 s_{1,2} - \Delta\lambda_2 s_{2,2} - \Delta\lambda_3 s_{3,2}) - (\sigma_3^B - \Delta\lambda_1 s_{1,3} - \Delta\lambda_2 s_{2,3} - \Delta\lambda_3 s_{3,3}) - \sigma_c^C \\ k(\sigma_1^B - \Delta\lambda_1 s_{1,1} - \Delta\lambda_2 s_{2,1} - \Delta\lambda_3 s_{3,1}) - (\sigma_2^B - \Delta\lambda_1 s_{1,2} - \Delta\lambda_2 s_{2,2} - \Delta\lambda_3 s_{3,2}) - \sigma_c^C \end{bmatrix} \quad (7.54) \\ &= \begin{bmatrix} 0 \\ 0 \\ 0 \end{bmatrix} \end{aligned}$$

where

$$\Delta\boldsymbol{\lambda} = \begin{bmatrix} \Delta\lambda_1 \\ \Delta\lambda_2 \\ \Delta\lambda_3 \end{bmatrix} \quad (7.55)$$

and the gradient matrix is given by

$$\frac{\partial \mathbf{F}}{\partial \Delta\boldsymbol{\lambda}^T} = \begin{bmatrix} -ks_{1,1} + s_{1,3} + d\sigma_c & -ks_{2,1} + s_{2,3} + d\sigma_c & -ks_{3,1} + s_{3,3} + d\sigma_c \\ -ks_{1,2} + s_{1,3} + d\sigma_c & -ks_{2,2} + s_{2,3} + d\sigma_c & -ks_{3,2} + s_{3,3} + d\sigma_c \\ -ks_{1,1} + s_{1,2} + d\sigma_c & -ks_{2,1} + s_{2,2} + d\sigma_c & -ks_{3,1} + s_{3,2} + d\sigma_c \end{bmatrix} \quad (7.56)$$

## 7.6 Consistent Constitutive Matrix

In the evaluation of the consistent constitutive matrix, the modification matrix aligned with the principal stresses,  $\hat{\mathbf{T}}$  is needed. The part related to the principal stresses,  $\bar{\mathbf{T}}$ , see equation (6.3), simplifies to the unit matrix

$$\bar{\mathbf{T}} = \begin{bmatrix} 1 & 0 & 0 \\ 0 & 1 & 0 \\ 0 & 0 & 1 \end{bmatrix} \quad (7.57)$$

because the derivative of  $\bar{\mathbf{b}}$  with respect to  $\bar{\boldsymbol{\sigma}}$  results in the zero-matrix

$$\frac{\partial \bar{\mathbf{b}}}{\partial \bar{\boldsymbol{\sigma}}} = \begin{bmatrix} 0 & 0 & 0 \\ 0 & 0 & 0 \\ 0 & 0 & 0 \end{bmatrix} \quad (7.58)$$

The part of  $\hat{\mathbf{T}}$ , that relates to the shear stresses,  $\tilde{\mathbf{T}}$ , is simply evaluated by equation (6.5). Thus it is possible to evaluate  $\hat{\mathbf{D}}^c$ . Afterwards, the consistent constitutive matrix aligned with the principal axes,  $\hat{\mathbf{D}}^{epc}$ , is calculated using either equation (5.23), (5.55) or (5.59), depending on the return algorithm used in finding the updated stress state.



# Computational Example: Strip Footing

To test the hardening Mohr-Coulomb model, a simple bearing capacity calculation of a strip footing is carried out in plane strain. This has been done by implementing the strain hardening Mohr-Coulomb model in FORTRAN and then utilizing it in a FEM-code written in MatLab, which rely on a Newton-Raphson procedure in the global equilibrium iterations, as shown in Table 5.1.

## 8.1 The Model

The model consists of a rigid rough foundation resting on top of a strain hardening Mohr-Coulomb material. Since a strip footing in plain strain is examined, advantage is made of the symmetry line of the problem, see Figure 8.1. The domain size is governed by  $L$  and  $H$ , which has been set to 30 m and 20 m respectively. The total width of the foundation is 2 m. The domain is meshed using 2-dimensional 6-node triangular linear strain elements utilizing a gaussorder of 6. The load of the foundation is modeled using a prescribed displacement of 1000 mm in the negative  $y$ -direction of the nodes situated directly under the foundation.

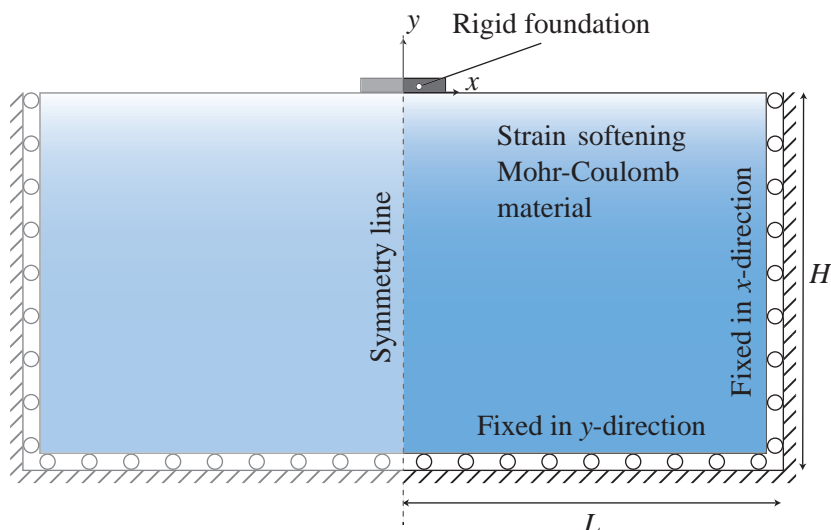


Figure 8.1: Sketch of the model of the foundation. Not to scale.

## 8.2 Material Parameters

The parameters of the Mohr-Coulomb material are found based on an approximation to a material with the Hoek-Brown parameters listed in Table 8.1.

State	GSI	$m_i$	$\sigma_{ci}$	$D$	$a$	$m_b$	$s$	$E$	$\nu$	$\gamma$
Peak	50	12	80 MPa	0	0.51	2.01	0.0039	9 GPa	0.25	20 kN/m <sup>3</sup>
Residual	25	12	80 MPa	0.5	0.53	0.34	0	9 GPa	0.25	20 kN/m <sup>2</sup>

Table 8.1: *Hoek-Brown material parameters of the peak and residual strength of the rock material at hand.*

As can be seen, for the peak strength of the rock material, intact rock is assumed,  $D = 0$ , with a uniaxial compressive strength of 80 MPa, a GSI value of 50 and a  $m_i$  constant of 12. For the residual strength, the GSI value is lowered to 25, and the disturbance factor,  $D$ , is set to 0.5. The Hoek-Brown constants  $a$ ,  $m_b$  and  $s$  are calculated based on equation (2.2)-(2.4). Young's modulus is assumed to be 9 GPa. The parameters originate from Sharan [2008] and the material associated with it is described as average quality rock mass, which according to Hoek and Brown [1997] should behave in a strain softening way. Further, the rock mass is assumed to have a specific weight,  $\gamma$ , of 20 kN/m<sup>3</sup>. Using the equations in chapter 3, the corresponding Mohr-Coulomb parameters can be seen in Table 8.2, where the general approach of equation (3.15) has been applied.

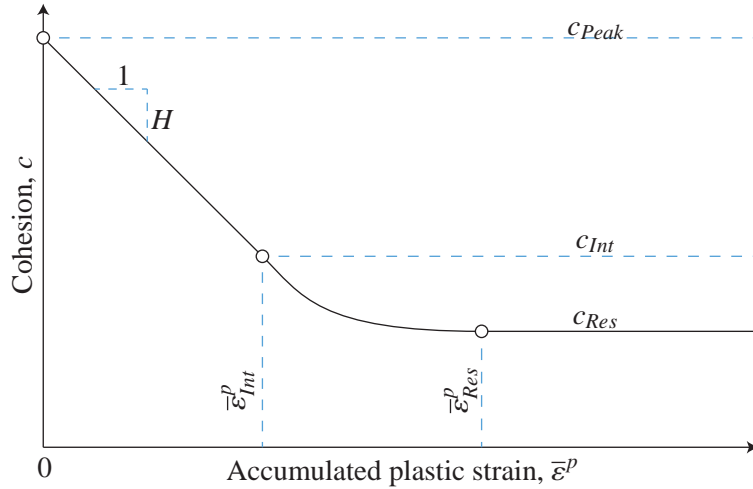
Parameter	$\varphi$	$c$
Peak	32.07°	4.21 MPa
Residual	17.93°	1.91 MPa

Table 8.2: *Mohr-Coulomb approximation of the Hoek-Brown parameters listed in Table 8.1. The approximation utilizes equation (3.15).*

Due to the restrictions of the current model, where only the cohesion changes during plastic loading, the model is unable to account for the change in friction angle. Because of this, the peak friction angle is used for the residual strength as well. In order to fully implement the strain softening behavior, it is also necessary to know how fast the strength drops. I.e. a relationship between the accumulated plastic strain and the cohesion. In the current example, this is modeled using three curve segments, as illustrated on Figure 8.2. The first segment consists of a linear softening curve with a constant slope of  $H$ , which is defined between the two points  $(0, c_{Peak})$  and the intermediate point  $(\bar{\varepsilon}_{Int}^p, c_{Int})$ . The second segment, defined between the intermediate point  $(\bar{\varepsilon}_{Int}^p, c_{Int})$  and the residual point  $(\bar{\varepsilon}_{Res}^p, c_{Res})$ , is modeled as a Bézier curve, with an initial slope of  $H$ , and an end slope of 0. The last segment defines a perfectly plastic behavior, once the residual strength is reached. This is done by modeling a line segment with a slope of 0, which extends to infinity. The intermediate cohesion,  $c_{Int}$ , is taken as

$$c_{Int} = c_{Res} + 0.3 \cdot (c_{Peak} - c_{Res}) \quad (8.1)$$

The intermediate and residual accumulated plastic strains,  $\bar{\varepsilon}_{Int}^p$  and  $\bar{\varepsilon}_{Res}^p$ , are varied, to study the influence on the results. For simplicity and numerical stability, associated plasticity is assumed. The final

Figure 8.2: Sketch of the  $\bar{\epsilon}^p$  –  $c$ -curve used in the example.

parameters used in the model are listed in Table 8.3. Further, two perfectly plastic cases are computed. Namely one where the strength is equal to the peak strength, and one where the strength is equal to the residual strength.

Parameter	$\varphi$	$c_{Peak}$	$c_{Int}$	$c_{Res}$	$\psi$
Value	$32.07^\circ$	4.21 MPa	2.60 MPa	1.91 MPa	$32.07^\circ$

Table 8.3: Material parameters used in the model.

### 8.3 Mesh Coarseness

In order to estimate the needed coarseness of the mesh, a convergence analysis has been performed on a model, where  $\bar{\epsilon}_{Int}^p$  and  $\bar{\epsilon}_{Res}^p$  have been set to 1 and 2 respectively. The mesh has then been generated with increasingly more degrees of freedom in order to estimate the influence on the peak and residual bearing capacity of the model. Based on this, a mesh coarseness is chosen, where further refinement only results in minor changes of the bearing capacity. As can be seen from Figure 8.3, the peak and residual bearing capacity is dependent upon the coarseness of the mesh. However, at around 10000 degrees of freedom, the bearing capacities start to stabilize, and only minor differences in the bearing capacities can be observed. Based on this, the model is meshed with 3825 elements, giving a total of 15692 degrees of freedom and 22950 gauss points. The mesh is shown in Figure 8.4.

### 8.4 Results

The load displacement curve for five different scenarios along with their  $\bar{\epsilon}^p$  –  $c$ -curves are shown in Figure 8.5 and Figure 8.6 respectively. The curves named “Perfectly Plastic Peak Strength” and “Per-

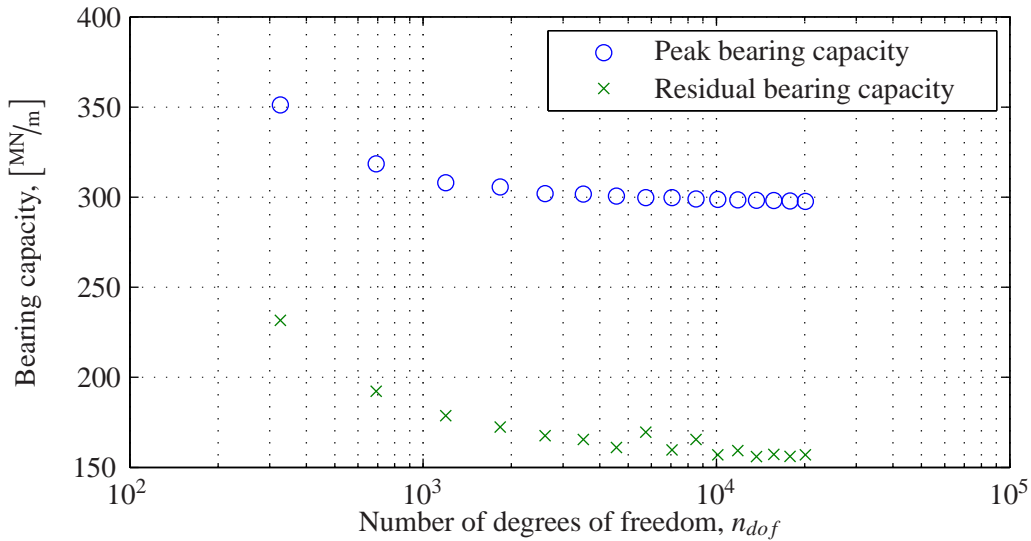


Figure 8.3: Convergence analysis of the peak and residual bearing capacity of a model with  $\bar{\epsilon}_{Int}^P = 1$  and  $\bar{\epsilon}_{Int}^P = 2$ .

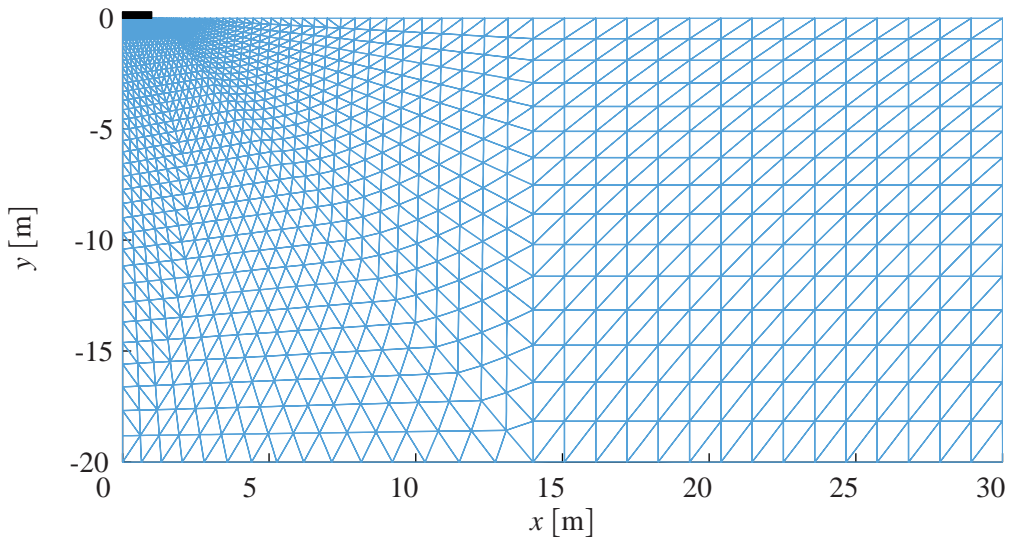


Figure 8.4: Mesh used in the current model, consisting of 3825 elements, 15692 degrees of freedom and 22950 gauss points.

fectly Plastic Residual Strength” are the perfectly plastic models using the peak and residual strength respectively, which give a load carrying capacity of  $309.2 \text{ MN/m}$  and  $141.6 \text{ MN/m}$ .

To verify these results, they are compared to the analytical solution given by Terzaghi’s bearing capacity formula

$$R = \frac{1}{2} \gamma b^2 N_y + q b N_q + c b N_c \quad (8.2)$$

where  $R$  is the bearing capacity,  $b$  is the foundation width,  $q$  is the overburden pressure and  $N_\gamma$ ,  $N_q$  and  $N_c$  are the dimensionless bearing capacity factors given by [Ovesen et al., 2007]

$$N_q = \exp(\pi \tan(\varphi)) \frac{1 + \sin(\varphi)}{1 - \sin(\varphi)} \quad (8.3)$$

$$N_\gamma = \frac{1}{4} ((N_q - 1) \cos(\varphi))^{3/2} \quad (8.4)$$

$$N_c = \frac{N_q - 1}{\tan(\varphi)} \quad (8.5)$$

Using the values of Table 8.3 together with equation (8.2), results in a peak and residual load carrying capacity of  $296.4 \text{ MN/m}$  and  $137.2 \text{ MN/m}$ . However, equation (8.2) is known to give a conservative bearing capacity, and thus, the perfectly plastic models seems to be in tune with the analytical solutions. The load carrying capacity of these models should mark the upper and lower bound of the expected load carrying capacity of the strain softening materials.

The three other curves of Figure 8.5 utilize strain softening, where the numbers indicate  $\bar{\varepsilon}_{Int}^p$  and  $\bar{\varepsilon}_{Res}^p$  respectively. The figure shows, that the strain softening materials never reach the load carrying capacity

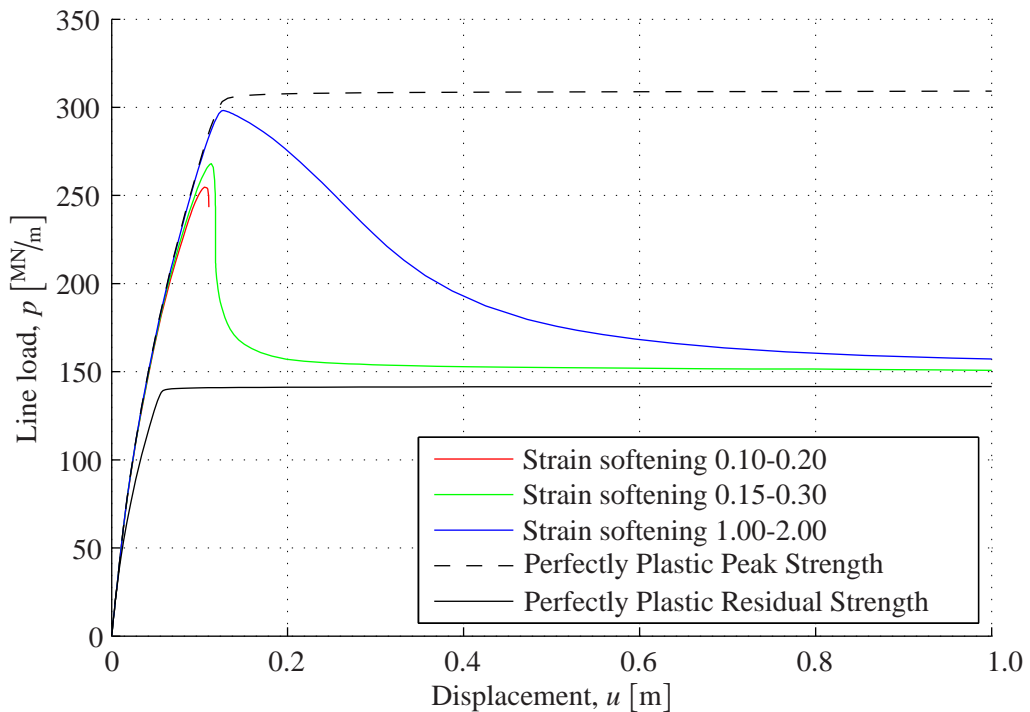


Figure 8.5: Load displacement curve of strip footing.  $u$  is the vertical displacement of the foundation. The numbers following the strain softening models are  $\bar{\varepsilon}_{Int}^p$  and  $\bar{\varepsilon}_{Res}^p$  respectively.

of the perfectly plastic model utilizing the peak strength. On the other hand, they do not approach the load carrying capacity of the perfectly plastic model utilizing the residual strength either. This seems realistic, since some gauss points reach plasticity before others and weakens, and thus should not be able to carry the peak load. Similarly, not all gauss points reach the residual strength in the model, and should thus be able to carry more than the residual load.

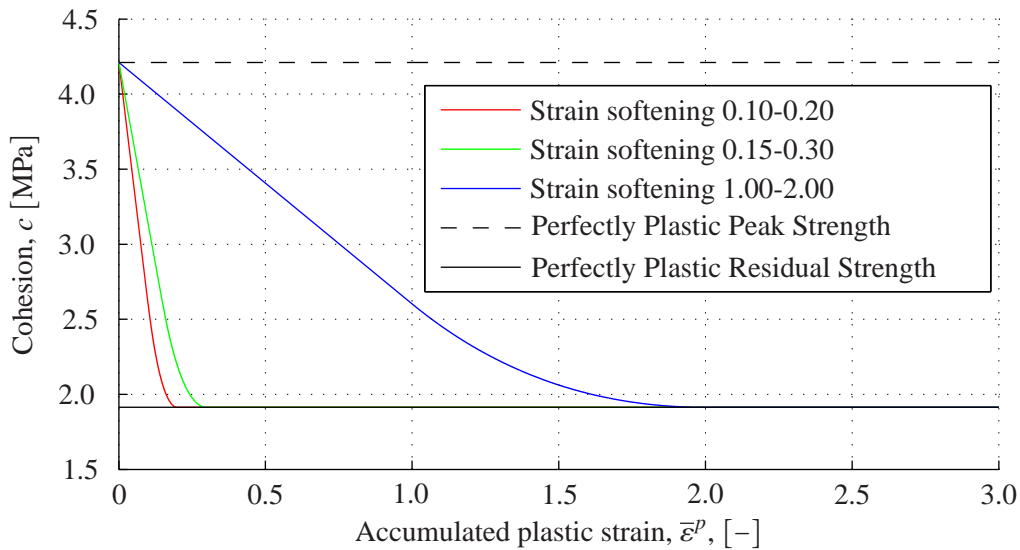


Figure 8.6: The strain softening behavior of the models shown in Figure 8.5.

Figure 8.7 shows the relationship between the residual accumulated plastic strain,  $\bar{\varepsilon}_{Res}^p$ , and the peak and residual bearing capacity of 12 different strain softening models, as well as the peak and residual strength of the perfectly plastic models. Together with Figure 8.5, it can be seen, that smaller

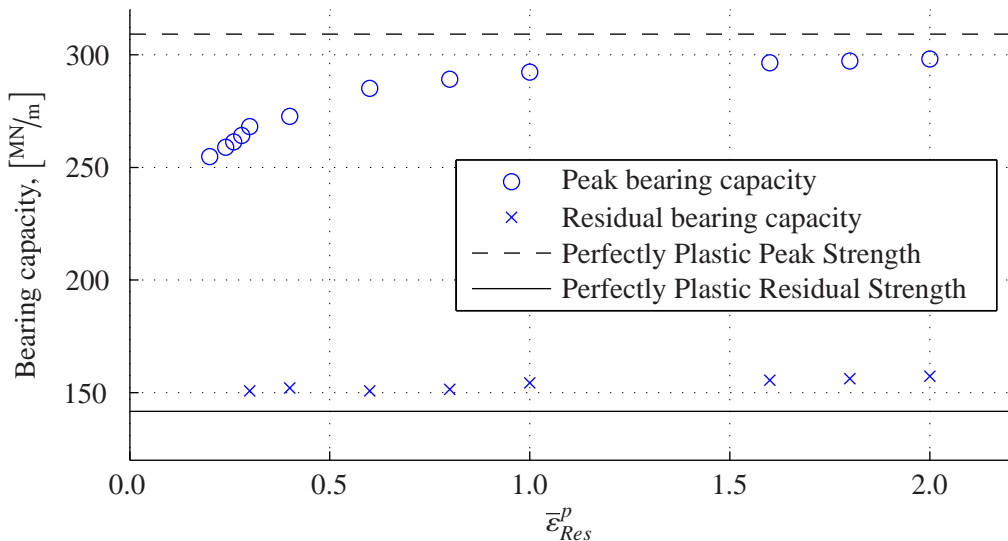


Figure 8.7: The peak and residual bearing capacity of 12 different strain softening models as a function of  $\bar{\varepsilon}^p$ . The bearing capacity of the perfectly plastic models is also shown.

$\bar{\varepsilon}_{Int}^p$  and  $\bar{\varepsilon}_{Res}^p$  result in a lower peak bearing capacity, as well as a more rapid decrease in the load carrying capacity towards a residual bearing capacity. The maximum load bearing capacity of the strain softening models is influenced by the choice of  $\bar{\varepsilon}_{Int}^p$  and  $\bar{\varepsilon}_{Res}^p$ . The 1.00–2.00 model predicts a maximum

bearing capacity of  $298.2 \text{ MN/m}$ , while the  $0.15 - 0.30$  model predicts a maximum bearing capacity of  $268.1 \text{ MN/m}$ , which is significantly less than that of the bearing capacity of the perfectly plastic model utilizing the peak strength. However, it is also almost twice the size of the bearing capacity of the perfectly plastic model using the residual strength. The  $1.00 - 2.00$  model predicts a residual bearing capacity of  $157.2 \text{ MN/m}$ , while the  $0.15 - 0.30$  model predicts a residual bearing capacity of  $150.8 \text{ MN/m}$ . An improvement compared to the bearing capacity of the perfectly plastic residual model of about 5 – 10 %. Thus, using the perfectly plastic model with the peak strength results in an unsafe model, while use of the residual strength results in a very conservative estimate of the bearing capacity.

Further, it is noticed, that the  $0.10 - 0.20$  model failed to converge, at some point just after the peak bearing capacity was reached, see Figure 8.5. The  $0.15 - 0.30$  model was the steepest model, which was found to converge. This is troublesome if even steeper drops in the load carrying capacity is needed. However, this might be solved by utilizing a more advanced global equilibrium iteration procedure than the standard Newton-Raphson. For example an arc-length method.

Figure 8.8 shows a plot of the cohesion throughout the soil of the  $0.15 - 0.30$  model, which shows, that the material located along the slip lines have reached the residual strength. This is consistent with the fact, that these zones experience the most plastic straining. The zones outside these slip lines are almost unaffected by the softening behavior.

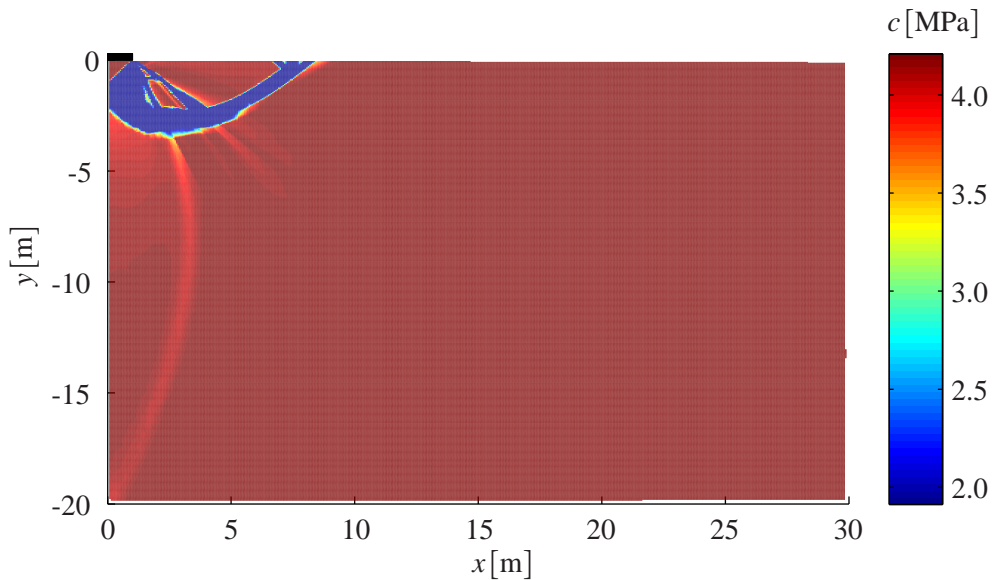


Figure 8.8: Plot of the cohesion throughout the soil at the end of the  $0.15-0.30$  model.

Figure 8.9 show a comparison of the accumulated plastic strains around the rupture zone of the model. The topmost graph shows the perfectly plastic model utilizing the peak strength, and the bottommost graph shows the perfectly plastic model utilizing the residual strength. The model in the middle is the strain softening  $0.15 - 0.30$  model. From the figure, it is seen, that the accumulated plastic strains of the softening model are more concentrated around the slip lines compared to the perfectly plastic models. This is probably due to the fact, that once plastic strains has developed in a point, the point weakens and thus further plasticity is more likely in this point, than in the neighboring material which surrounds it.

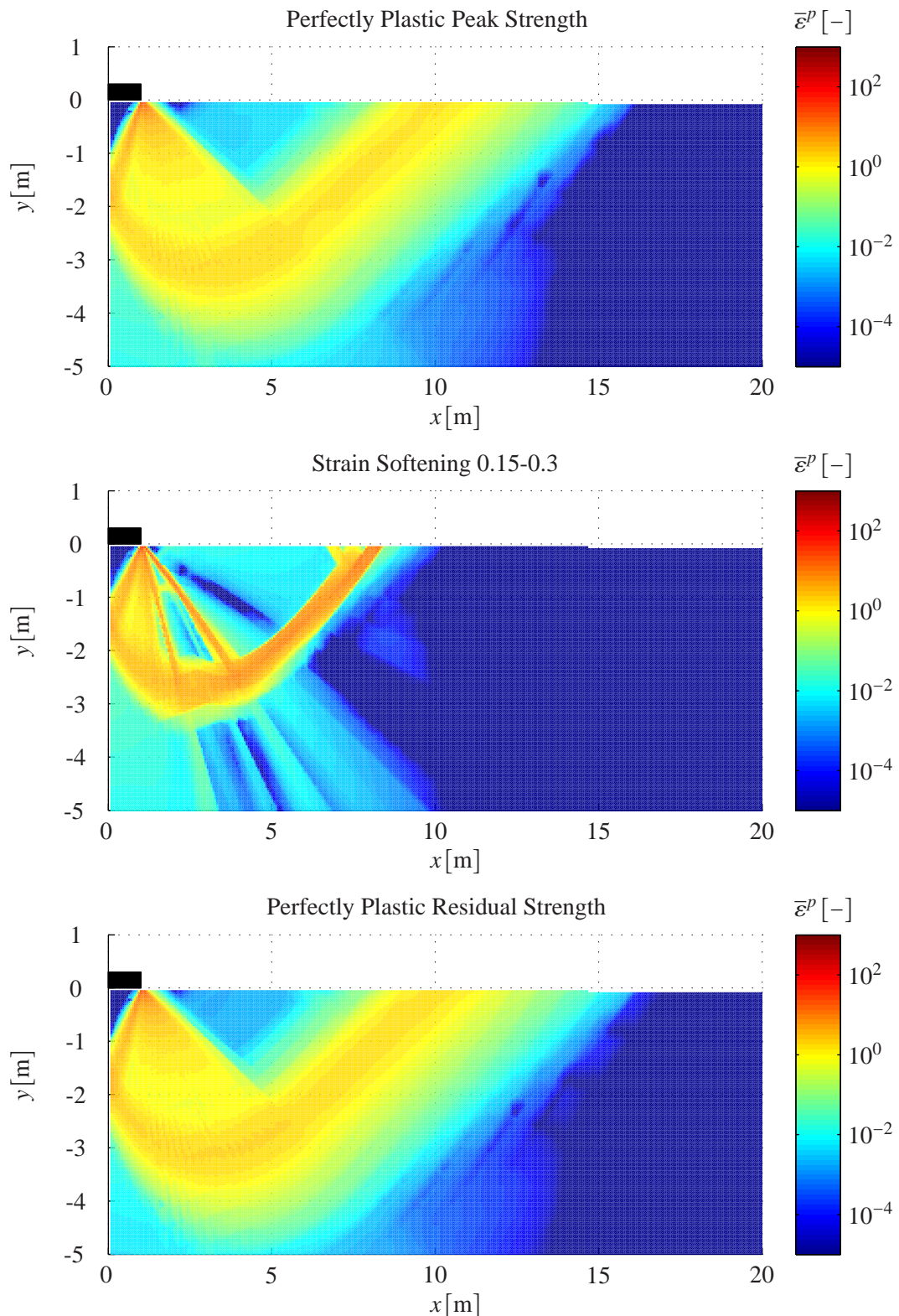


Figure 8.9: Plot of the accumulated plastic strain throughout the soil of the perfectly plastic peak strength model, strain softening 0.15-0.30 model and perfectly plastic residual strength model.

# Computational Example: Tunnel Excavation

To further test the approach, a tunnel excavation is carried out using an axisymmetric model, where the purpose is to estimate the tunnel wall displacement as well as the plastic zone.

## 9.1 The model

The idea behind the model is to simulate a tunnel excavation in an infinite rock mass. This is done by reducing the pressure,  $p$ , on the tunnel wall, from the in situ stress state,  $p_{\text{inf}}$ , to zero, see Figure 9.1, and record the ensuing tunnel wall displacement. The radius of the tunnel is given by  $r_T$ , which has been set to 2,5 m. The tunnel axis is aligned in the z-direction.

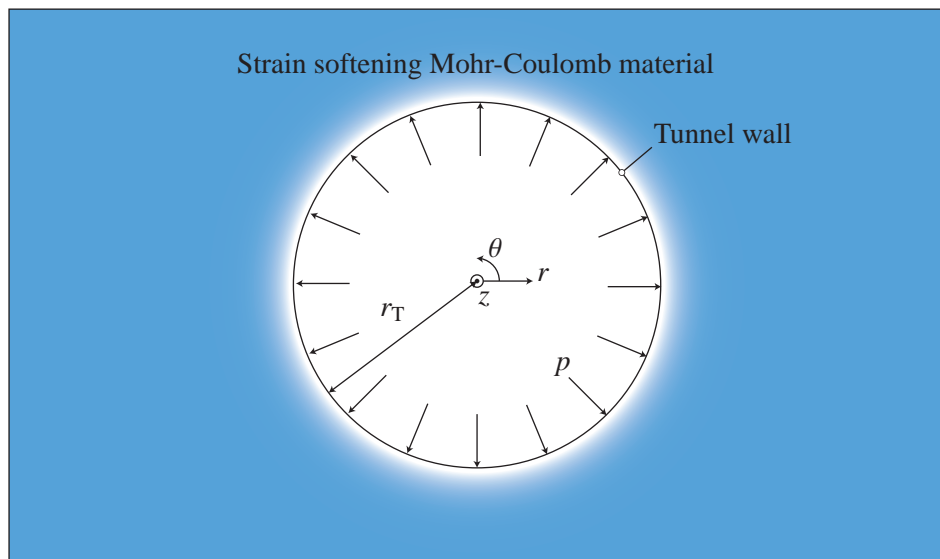


Figure 9.1: Concept of the tunnel model.

The axisymmetric properties of the problem is utilized, and a 1 m section of the tunnel in the  $z$ -direction is modeled, see Figure 9.2. Further, the infinite rock mass is bounded by a domain with a radius of  $r_{\text{BC}}$ , which has been set to 50 m in the example at hand. As with the example in chapter 8, the

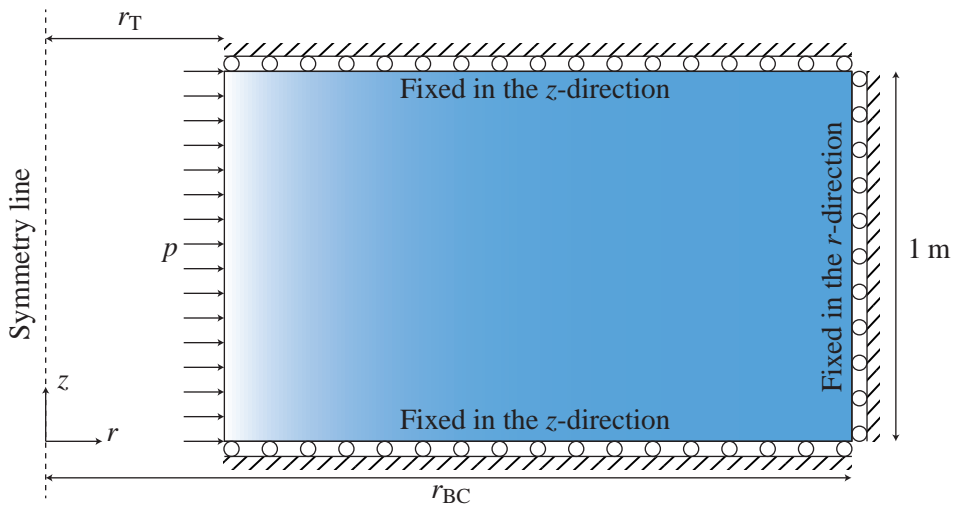


Figure 9.2: Sketch of the tunnel model.

mesh is generated with 2-dimensional 6-node triangular linear strain elements.

## 9.2 Material Parameters

The model tries to simulate an excavation in rock material with the Hoek-Brown parameters listed in Table 9.1.

State	GSI	$m_i$	$\sigma_{ci}$	$D$	$a$	$m_b$	$s$	$E$	$\nu$	$\gamma$
Peak	30	8	20 MPa	0	0.52	0.66	0.0004	1.4 GPa	0.3	26 kN/m <sup>3</sup>
Residual	15	8	20 MPa	0.5	0.56	0.14	0	1.4 GPa	0.3	26 kN/m <sup>2</sup>

Table 9.1: Hoek-Brown material parameters of the peak and residual strength of the rock material at hand.

The parameters of the peak strength are taken from Sharan [2008], which describe the rock material as very poor. According to Hoek and Brown [1997], very poor rock material tends to behave perfectly plastic. However, in the current example, it is assumed that the material softens during plastic straining. Thus the residual strength is found in much the same way as it was done in chapter 8. Namely by reducing the GSI-value to half of the original value and setting the disturbance factor to 0.5.

Assuming the excavation takes place 100 m below the surface and using the approximations of chapter 3 along with the estimate of  $\sigma_{3,max}$  based on deep tunnels, equation (3.12), the Mohr-Coulomb parameters listed in Table 9.2 are obtained.

Parameter	$\varphi$	$c$
Peak	33.74°	256 kPa
Residual	19.28°	103 kPa

Table 9.2: *Mohr-Coulomb approximation of the Hoek-Brown parameters listed in Table 8.1.*  
*The approximation utilizes equation (3.12).*

Similarly to the example of the strip footing, the friction angle of the model is taken to be given by the peak friction angle, and the softening behavior is modeled according to Figure 8.2 and equation (8.1). Thus, the final material parameters are given in Table 9.3.

Parameter	$\varphi$	$c_{Peak}$	$c_{Int}$	$c_{Res}$	$\psi$
Value	33.74°	256 kPa	149 kPa	103 kPa	33.74°

Table 9.3: *Material parameters used in the model.*

The in situ stress state of the rock mass,  $p_{inf}$ , is assumed to be a hydrostatic pressure, given by the depth, and the unit weight of the rock

$$p_{inf} = 26 \text{ kN/m}^3 \cdot 100 \text{ m} = 2.6 \text{ MPa} \quad (9.1)$$

The effects of gravity are neglected in the model. Similarly to the example of the strip footing, the model is tried with different values of the intermediate and residual accumulated plastic strain,  $\bar{\varepsilon}_{Int}^p$  and  $\bar{\varepsilon}_{Res}^p$ , as well as two perfectly plastic cases with the peak and residual strength respectively.

## 9.3 Mesh Coarseness

Similar to the example of chapter 8, a convergence analysis has been made in order to find an appropriate mesh coarseness. This has been done with a model where  $\bar{\varepsilon}_{Int}^p = 0.025$  and  $\bar{\varepsilon}_{Res}^p = 0.050$ . The tunnel wall displacement as a function of the number of degrees of freedom is shown in Figure 9.3. From this figure it is seen, that only minor changes in the wall displacement is found once the number of degrees of freedom is above 10000. Based on this, the model is meshed using 4800 elements, resulting in 28800 gauss points and 19602 degrees of freedom. The mesh can be seen in Figure 9.4.

## 9.4 Results

The load displacement curve of the tunnel wall of eight models is shown in Figure 9.5 together with a close up in Figure 9.6. The strain softening behavior of the models can be seen on Figure 9.7. From the figures, it is seen that the perfectly plastic model using the peak strength gives a tunnel wall displacement of 30 mm, while the model using the residual strength gives a displacement of 126 mm. Using the analytical solution for the perfectly plastic case presented in Carranza-Torres [2003], the tunnel wall displacement is found to be 30.5 mm and 130 mm respectively, which suggests that the finite element model is sound. All of the strain softening models predict wall displacements in between the two perfectly plastic models, which is what was expected. Further, the extent of the plastic zone,

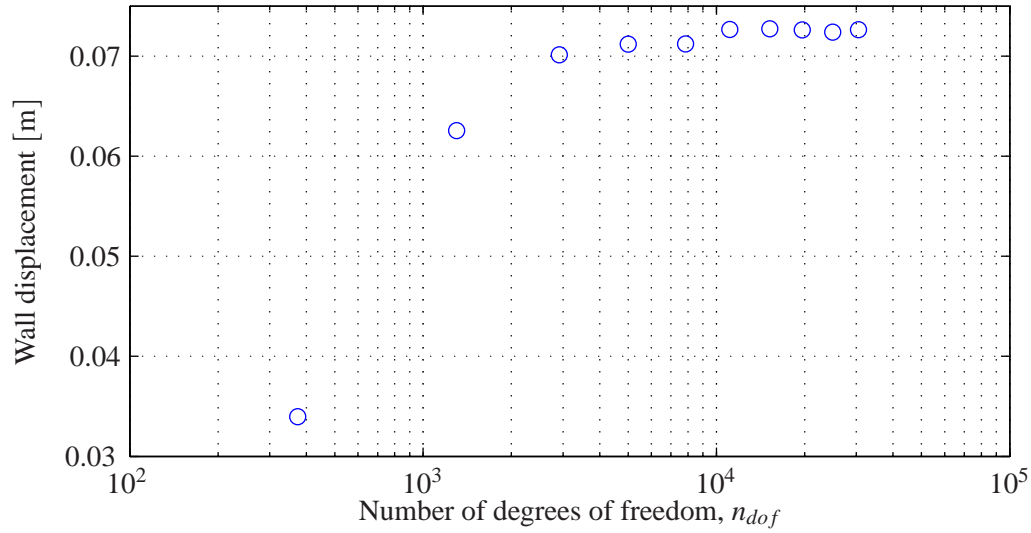


Figure 9.3: *Displacement of the tunnel wall as a function of the number of degrees of freedom of a model with  $\bar{\varepsilon}_{Int}^P = 0.025$  and  $\bar{\varepsilon}_{Res}^P = 0.050$ .*

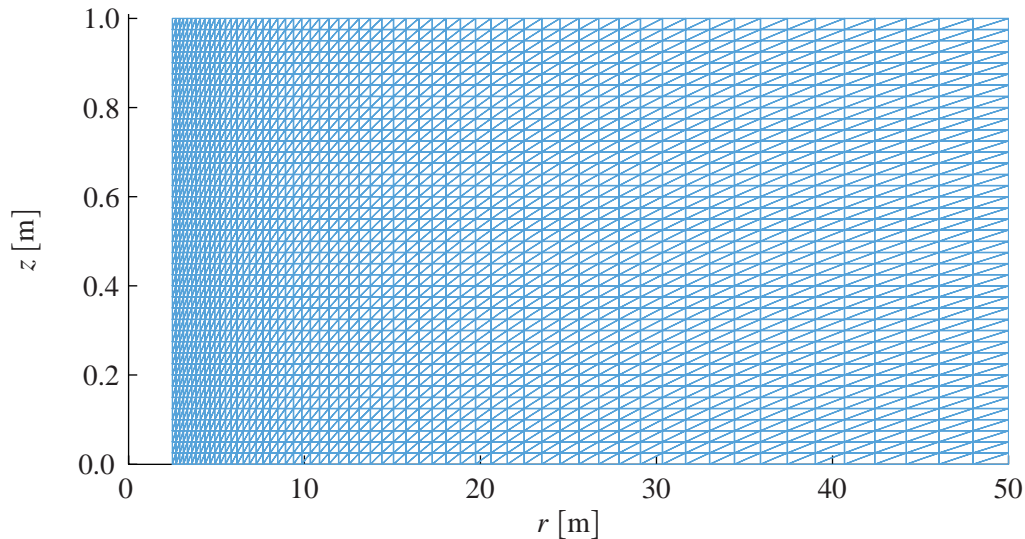


Figure 9.4: *Mesh used in the current model, consisting of 4800 elements, 19602 degrees of freedom and 28800 gauss points.*

sketched in Figure 9.8, ranges from 4.12 m for the peak strength model to 5.8 m for the residual strength model as shown in Figure 9.9. The analytical solution of Carranza-Torres [2003] results in plastic zones of 4.11 m and 5.72 m for the perfectly plastic peak and residual models.

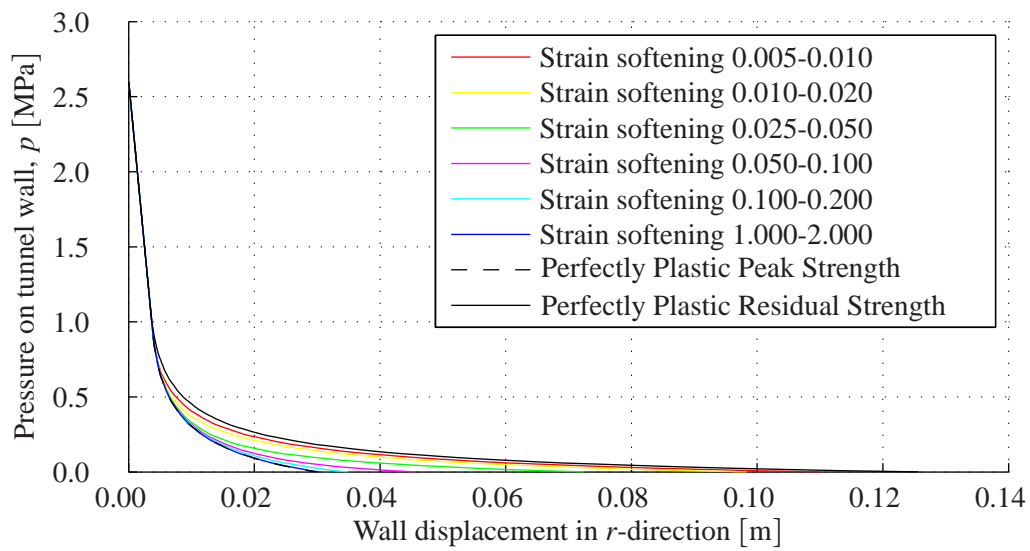


Figure 9.5: Displacement of the tunnel wall. The numbers following the strain softening models are  $\bar{\varepsilon}_{Int}^P$  and  $\bar{\varepsilon}_{Res}^P$  respectively.

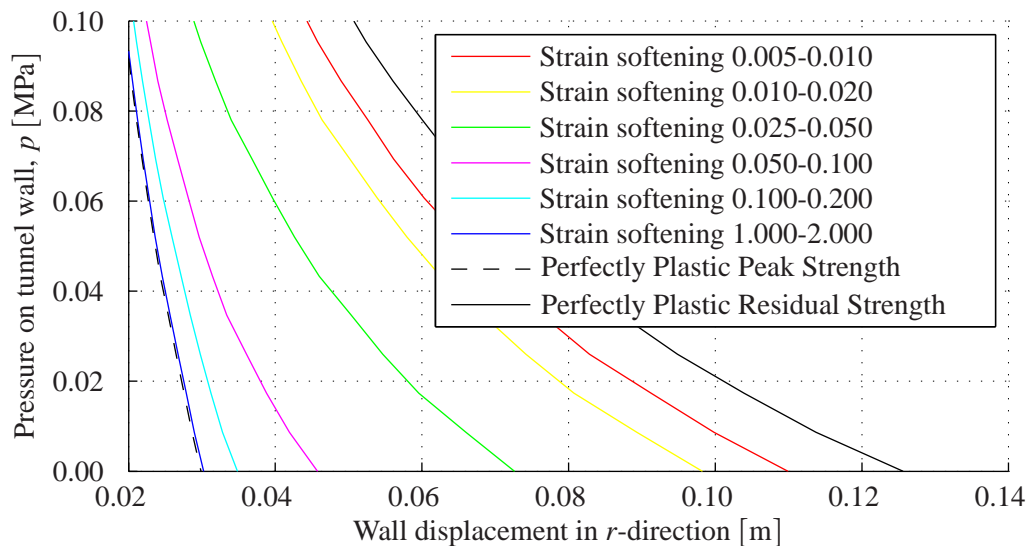


Figure 9.6: Close up of Figure 9.5.

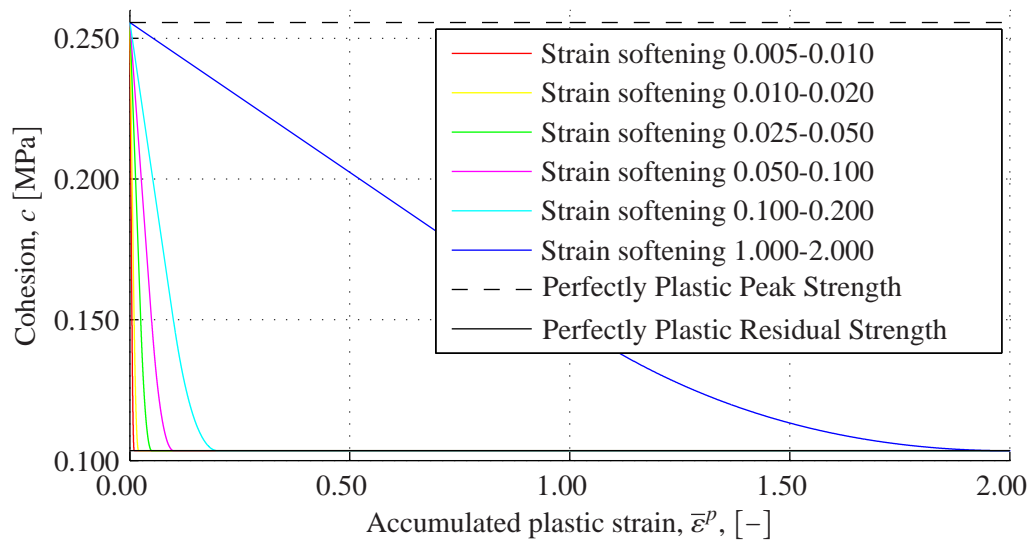


Figure 9.7: The strain softening behavior of the models.

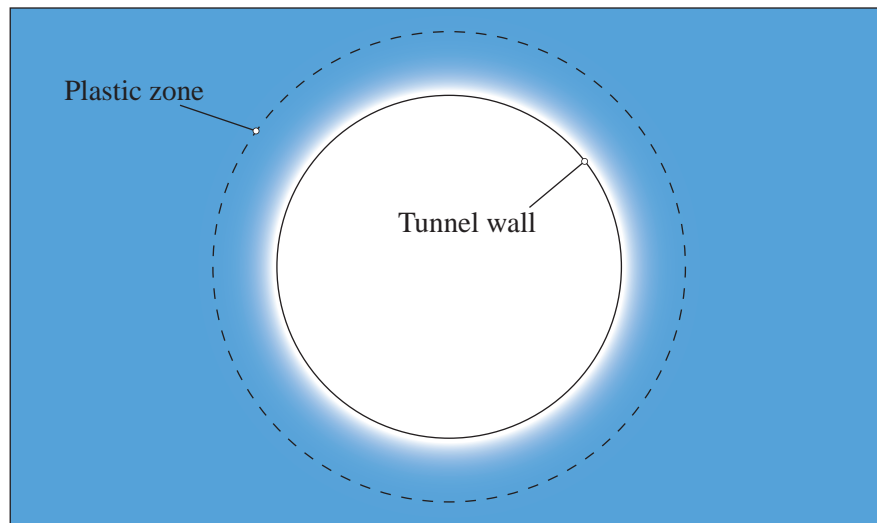


Figure 9.8: Illustration of the extent of the plastic zone.

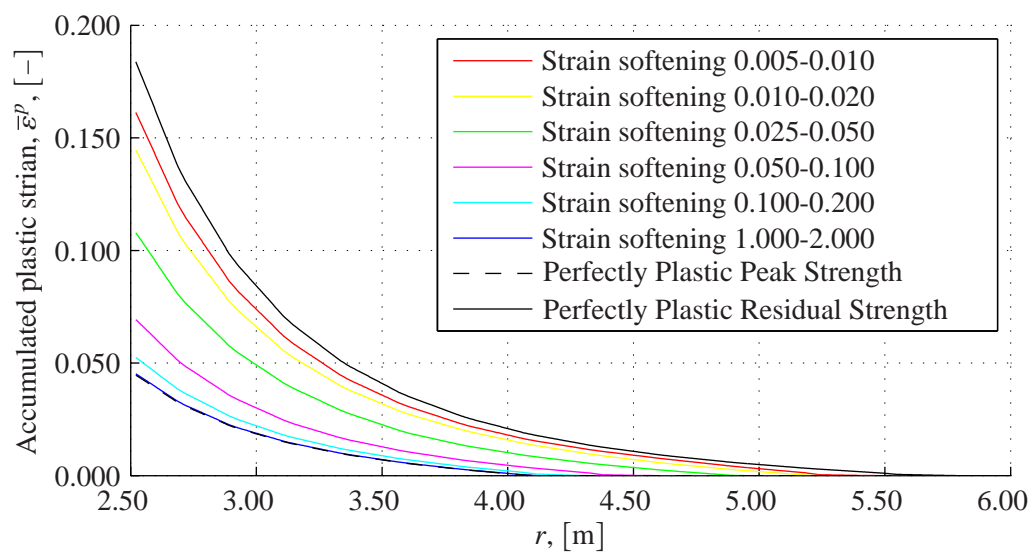


Figure 9.9: The extent of the plastic zone of the models.



---

## Conclusion

The successful derivation and implementation of the strain hardening Mohr-Coulomb criterion described in chapter 7 shows, that it is possible to make use of return mapping in principal stress space for materials, which exhibit hardening/softening properties.

The proof-of-concept examples of the strip footing and tunnel excavation show the expected results, where the strain softening materials result in solutions somewhere in between the two extremities of the perfectly plastic models using the peak and residuals strengths. Thus the hardening properties allow for a more detailed description of the problem at hand, which should result in a more safe solution, than a model utilizing perfect plasticity along with the peak strength, as well as less conservative solution than a model utilizing perfect plasticity along with the residual strength.

Since the implemented model can handle any arbitrary development of the cohesion during plastic straining, it should be applicable to a great deal of problems. However, as is evident from the examples, approximations to the Hoek-Brown parameters with a Mohr-Coulomb failure criterion suggest, that the friction and dilation angles change during plastic straining as well. Something that the current model is unable to account for.

To further test the use of hardening properties along with principal stress updating schemes, a more advanced constitutive model, utilizing several hardening and state parameters could be developed. For example a Mohr-Coulomb model, where the friction and dilation angles are dependent of the state parameters of the material. Moreover, the expressions for the consistent constitutive matrix of two and three active yield surfaces, equation (5.55) and (5.59), together with return mapping in principal stress space, allows for a fairly straight forward way of developing a hardening Hoek-Brown model, which eliminate the need for the Mohr-Coulomb approximation of hardening rock material.

Next step would be to implement these models into commercial finite element programs, in order to be truly useful for the professional engineering community, which require ease of use and accessibility.



---

# Bibliography

- Carlos Carranza-Torres. Dimensionless graphical representation of the exact elasto-plastic solution of a circular tunnel in a mohr-coulomb material subject to uniform far-field stresses. *Rock Mechanics and Rock Engineering*, 36:237–253, 2003.
- Johan Clausen. *Efficient Non-Linear Finite Element Implementation of Elasto-Plasticity for Geotechnical Problems*. PhD thesis, Aalborg University, 2007.
- Johan Clausen, Lars Damkilde, and Lars Andersen. Efficient return algorithms for associated plasticity with multiple yield planes. *International Journal For Numerical Methods In Engineering*, 66:1036–1059, 2006.
- Robert D. Cook, David S. Malkus, Michael E. Plesha, and Robert J. Witt. *Concepts and Applications of Finite Element Analysis*. John Wiley & Sons, Ltd., 2002.
- Michael Anthony Crisfield. *Non-Linear Finite Element Analysis*. John Wiley & Sons, Ltd., 2000.
- Eduardo de Souza Neto, Djordje Peric, and David Owens. *Computational Methods for Plasticity - Theory and Applications*. John Wiley & Sons, Ltd., 2008.
- Evert Hoek. *Practical Rock Engineering*. 2007.
- Evert Hoek and Edwin T. Brown. Practical estimates of rock mass strength. *International Journal of Rock Mechanics & Mining Sciences*, 34, No. 8:1165–1186, 1997.
- Evert Hoek and Mark S. Diederichs. Empirical estimation of rock mass modulus. *International Journal of Rock Mechanics & Mining Sciences*, 43:203–215, 2006.
- Evert Hoek, Carlos Carranza-Torres, and Brent Corkum. Hoek-Brown failure criterion - 2002 edition, 2002.
- Warner Tjardus Koiter. Stress-strain relations, uniqueness and variational theorems for elasto-plastic materials with a singular yield surface. *Quarterly of applied mathematics.*, 11:350–354, 1953.
- Paul Marinos and Evert Hoek. GSI: A geologically friendly tool for rock mass strength estimation. In *Proceedings of the International Conference on Geotechnical and Geological Engineering, Geo-Eng2000*, 2000.

- Richard S. Merifield, Andrei V. Lyamin, and Scott W. Sloan. Limit analysis solutions for the bearing capacity of rock masses using the generalised Hoek-Brown criterion. *International Journal of Rock Mechanics & Mining Sciences*, 43:920–937, 2006.
- Joop C. Nagtegaal. On the implementation of inelastic constitutive equations with special reference to large deformation problems. *Computer Methods in Applied Mechanics and Engineering*, 33:469–484, 1982.
- Niels Saabye Ottosen and Matti Ristinmaa. *The Mechanics of Constitutive Modeling*. Elsevier Ltd, 2005.
- Niels Krebs Ovesen, Leif Fuglsang, Gunnar Bagge, Anette Krogsbøll, Carsten S. Sørensen, Bent Hansen, Klaus Bødker, Lotte Thøgersen, Jens Galsgaard, and Anders H. Augustesen. *Lærebog i Geoteknik*. Polyteknisk Forlag, 2007.
- Rocscience Inc. Roclab - user's guide, 2007.
- Shailendra K. Sharan. Analytical solutions for stresses and displacements around a circular opening in a generalized Hoek-Brown rock. *International Journal of Rock Mechanics & Mining Sciences*, 45: 78–85, 2008.
- Emil Smed Sørensen. Modified generalised Hoek-Brown model, 2012. Aalborg University, M.Sc. 3rd semester report.



